(12) INTERNATIONAL APPLICATION PUBLISHED UNDER THE PATENT COOPERATION TREATY (PCT)

(19) World Intellectual Property Organization
International Bureau

(43) International Publication Date
20 October 2016 (20.10.2016)

WIPO | PCT

(10) International Publication Number
WO 2016/166232 A1

(51) International Patent Classification:
G01N 33/68 (2006.01) *G01N 33/487* (2006.01)

(21) International Application Number:
PCT/EP2016/058252

(22) International Filing Date:
14 April 2016 (14.04.2016)

(25) Filing Language: English

(26) Publication Language: English

(30) Priority Data:

1506307.6	14 April 2015 (14.04.2015)	GB
1507264.8	29 April 2015 (29.04.2015)	GB

(71) Applicants: **KATHOLIEKE UNIVERSITEIT LEUVEN** [BE/BE]; KU Leuven Reseach & Development, Waaistraat 6 - Box 5105, B-3000 Leuven (BE). **RIJKSUNIVERSITEIT GRONINGEN** [NL/NL]; Broerstraat 5, NL 9712 CP Groningen (NL).

(72) Inventors: **MAGLIA, Giovanni**; Carry van Bruggenweg 53, 9408 DX Assen (NL). **SOSKINE, Mikhael**; De Drift 20-5, 9203 GH Drachten (NL). **BIESEMANS, Annemie**; Edelzangerslaan 40, 8, 3010 Kessel-Lo (BE). **VAN MEERVELT, Veerle**; Matantjesstraat 10, 3220 Holsbeek (BE). **POOLMAN, Bert**; Botanicuslaan 8, 9751 AC Haren (NL). **SCHUURMAN-WOLTERS, Gea**; JP Santeeweg 92, 9312 TB Nietap (NL).

(74) Agent: **IPLODGE BVBA**; Technologielaan 9, B-3001 Heverlee (BE).

(81) Designated States *(unless otherwise indicated, for every kind of national protection available)*: AE, AG, AL, AM, AO, AT, AU, AZ, BA, BB, BG, BH, BN, BR, BW, BY, BZ, CA, CH, CL, CN, CO, CR, CU, CZ, DE, DK, DM, DO, DZ, EC, EE, EG, ES, FI, GB, GD, GE, GH, GM, GT, HN, HR, HU, ID, IL, IN, IR, IS, JP, KE, KG, KN, KP, KR, KZ, LA, LC, LK, LR, LS, LU, LY, MA, MD, ME, MG, MK, MN, MW, MX, MY, MZ, NA, NG, NI, NO, NZ, OM, PA, PE, PG, PH, PL, PT, QA, RO, RS, RU, RW, SA, SC, SD, SE, SG, SK, SL, SM, ST, SV, SY, TH, TJ, TM, TN, TR, TT, TZ, UA, UG, US, UZ, VC, VN, ZA, ZM, ZW.

(84) Designated States *(unless otherwise indicated, for every kind of regional protection available)*: ARIPO (BW, GH, GM, KE, LR, LS, MW, MZ, NA, RW, SD, SL, ST, SZ, TZ, UG, ZM, ZW), Eurasian (AM, AZ, BY, KG, KZ, RU, TJ, TM), European (AL, AT, BE, BG, CH, CY, CZ, DE, DK, EE, ES, FI, FR, GB, GR, HR, HU, IE, IS, IT, LT, LU, LV, MC, MK, MT, NL, NO, PL, PT, RO, RS, SE, SI, SK, SM, TR), OAPI (BF, BJ, CF, CG, CI, CM, GA, GN, GQ, GW, KM, ML, MR, NE, SN, TD, TG).

[Continued on next page]

(54) Title: NANOPORES WITH INTERNAL PROTEIN ADAPTORS

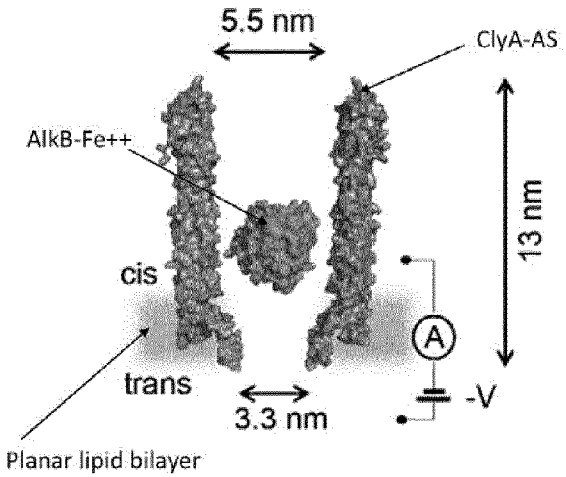

Figure 1

(57) Abstract: The present invention relates to methods for detecting an analyte in a sample, comprising the steps of obtaining a nanopore sensor comprising a nanopore and a protein adaptor internalized in the lumen of the nanopore, adding a sample comprising an analyte to the cis side or the trans side of the nanopore, and measuring conductance across the nanopore, wherein a change in conductance after adding the sample indicates the analyte is present in the sample and has bound to the protein adaptor. The present invention equally relates to nanopore sensors comprising a nanopore and a protein adaptor internalized in the lumen of the nanopore. Herein the protein adaptor is a functional enzyme or ligand-binding protein.

WO 2016/166232 A1

Published:

— *with international search report (Art. 21(3))*

— *with sequence listing part of description (Rule 5.2(a))*

NANOPORES WITH INTERNAL PROTEIN ADAPTORS

FIELD OF INVENTION

The present invention relates to nanopore sensors comprising nanopore proteins and protein adaptors internalized in the lumen of the nanopores. The protein adaptor retains both its binding specificity for specific substrates and its functional activity, so that the nanopore sensor may be used for detecting analytes and characterizing unique properties of bound analytes.

BACKGROUND

Over the past two decades nanopore analysis has emerged as a promising analytical tool for single-molecule analysis [Howorka, S. & Siwy, Z. (2009) *Chem Soc Rev* **38**, 2360-2384; Bayley, H. (2015) *Clin. chem.* **61**, 25-31; Luchian, T et al. (2003) *Angew. Chem.* **42**, 3766-3771; Bezrukov, S. M. et al. (1994) *Nature* **370**, 279-281]. Nanopore technology allows the investigation of native molecules with high sampling bandwidth without the need for labelling, chemical modifications or surface immobilisation. Further, the ionic current output signal can be easily interfaced with miniaturised and portable electronic devices. For instance, arrays of nanopores integrated into a MinION™ sequencer have been recently used for the profiling of genomic DNA [Ashton, P. M. et al. (2014) *Nat. Biotechnol.* **33**, 296–300; Mikheyev, A. S. & Tin, M. M. (2014) *Mol. ecol. res.* **14**, 1097-1102; Quick, J. et al. (2014) *GigaScience* **3**, 22.]. Furthermore, biological nanopores have been reconstituted into bilayers formed on glass nanopipettes (White, R. J. et al (2007). *J Am Chem Soc* **129**, 11766-11775) and on glass tips for scanning ion-conductance microscopy (Zhou, Y. et al (2014) Langmuir 30, 15351-15355). Therefore, nanopore-functionalized nanopipettes that can detect and quantify metabolites are promising platforms for measurement in single cells.

Previous studies showed that small molecules binding to cyclodextrin (Gu, L. Q. et al. (1999) *Nature* **398**, 686-690) and cyclic peptide adaptors (Sanchez-Quesada, (2000) J. Am. Chem. Soc. **122**, 11757-11766) or cucurbiturils carriers (Braha, O. et al. (2005) *Chemphyschem*, **6**, 889-892). ("guest adaptors") could be detected by ionic current recordings using the α-hemolysin (αHL) nanopore. However, these guest adaptors and carriers do not bind selectively to host molecules, complicating the identification of specific analytes, especially in a complex mixture of compounds like a biological sample. Thus, there remains a need in the art for new nanopore sensors that confer highly-selective binding to target analytes.

It is well-known that proteins bind selectively to targets, and a further study demonstrated that electroosmotic and electrophoretic forces allow small proteins such as thrombin to become trapped inside nanopores [Soskine, M. et al. (2013) *J Am Chem Soc*, **135**, 13456-13463; Soskine, M. (2012) *Nano Lett.* **12**, 4895-4900], suggesting that proteins might be used as adaptors inside nanopores. However, building such hybrid devices is challenging. Most proteins are too large to be incorporated into the αHL and other biological nanopores [Jung, Y. et al. (2005) *Biochem.* **44**, 8919-8929; Movileanu, L. (2000) *Nat. Biotechnol.* **18**, 1091-1095. Fahie, M. et al. (2015) *ACS nano*, **9**, 1089-1098] and translocate through solid-state nanopores too fast to be properly sampled (Plesa, C. et al. (2013) *Nano Lett.*, **13**, 658-663). Moreover, analysis in solid-state nanopores indicates that proteins would not be expected to retain their structure or function in the lumen of a nanopore. In solid-state nanopores, proteins are stretched by an electrical field (Oukhaled, A. et al. (2011) *ACS nano* **5**, 3628-3638) and unfolded under applied potentials higher than +200 mV (Freedman, K. J. (2013). *J. Scientific reports* **3**, 1638). If proteins are stretched or unfolded, their target binding sites and function are likely lost.

SUMMARY OF INVENTION

Described herein is a nanopore sensor based on a nanopore and a protein adaptor that is internalized in the lumen of the nanopore. Different types of proteins, including enzymes, can be used. The protein adaptor remains in the lumen of the nanopore without the use of covalent chemistry or other immobilization techniques, and surprisingly, the protein adaptor retains its folded structure, function and/or binding properties. The binding of analytes to the internalized protein adaptor is reflected by changes in the nanopore conductance. Accordingly, methods for detecting analytes using the sensor are also described, and uses of the sensor in the discovery of new therapeutics and the detection of biomarker analytes in biological samples is disclosed.

A first aspect of the present invention relates to a nanopore sensor comprising a nanopore and a protein adaptor internalized in the lumen of the nanopore, wherein the protein adaptor is a functional enzyme or ligand-binding protein.

In some embodiments, a first opening in the nanopore has a wider diameter than a second opening in the nanopore.

In certain embodiments, the nanopore sensor is cytolysin A (ClyA) or a mutant or variant thereof.

In some embodiments, the protein adaptor is globular. The protein adaptor may be a functional enzyme selected from a demethylase and a reductase. In certain

embodiments, the protein adaptor comprises a tag. The tag may have a net overall positive or negative charge.

In certain embodiments, the protein adaptor forms a complex with one or more additional molecules. In some embodiments, the protein adaptor binds to a target analyte. The target analyte may be selected from a small molecule analyte, a protein analyte, and a nucleic acid analyte. In some embodiments, the target analyte is charged.

In some embodiments, the nanopore sensor is ClyA, and comprises a plurality of subunits, each subunit comprising an amino acid sequence represented by SEQ ID NO:3.

In certain embodiments, the nanopore sensor is a demethylase, for example, AlkB demethylase. In certain embodiments, the nanopore sensor is a reductase, for example, dihydrofolate reductase. In a specific embodiment the demethylase is AlkB demethylase comprising an Asn120Asp mutation.

Anotherr aspect of the present invention relates to methods for detecting an analyte in a sample, comprising the steps of:

a) obtaining a nanopore sensor comprising a nanopore and a protein adaptor internalized in the lumen of the nanopore, wherein the protein adaptor is a functional enzyme or ligand-binding protein.

b) adding a sample comprising an analyte to the *cis* side or the *trans* side of the nanopore, and

c) measuring conductance across the nanopore, wherein a change in conductance after addition of the sample indicates the binding of the analyte to the protein adaptor and the presence of the analyte in the sample.

The present invention thus discloses a method for detecting an analyte in a sample, comprising (a) obtaining a nanopore sensor comprising a nanopore and a protein adaptor internalized in the lumen of the nanopore, (b) adding the sample to the *cis* side or the *trans* side of the nanopore, and (c) measuring conductance across the nanopore, wherein a change in conductance after adding the sample indicates the analyte is present in the sample and has bound to the protein adaptor.

The present invention thus discloses a method for identifying a ligand for a protein adaptor, comprising (a) obtaining a nanopore sensor comprising a nanopore and a protein adaptor internalized in the lumen of the nanopore, (b) adding a test compound to the *cis* side or the *trans* side of the nanopore, and (c) measuring the conductance across the nanopore, wherein a change in conductance after adding the test compound indicates that the test compound is a ligand that binds to the protein adaptor.

Herein the nanopore has a first and a second opening whereby the first opening has a wider diameter than the second opening.

In specific embodiments, the nanopore is cytolysin A (ClyA) or a mutant or variant thereof such as cytolysin A (ClyA) mutant Gln56Trp.

In specific embodiments, ClyA comprises a plurality of subunits, each subunit comprising an amino acid sequence represented by SEQ ID NO:3.

In specific embodiments, the protein adaptor is globular.

In specific embodiments , wherein the protein adaptor is a demethylase enzyme or a reductase enzyme, such as AlkB demethylase (for example AlkB demethylase comprising an Asn120Asp mutation) or dihydrofolate reductase.

In specific embodiments the protein adaptor comprises a tag, which may have a net overall positive or negative charge.

In specific embodiments wherein the protein adaptor forms a complex with one or more additional molecules.

In specific embodiments the analyte is a small molecule, a protein, or a nucleic acid.

In specific embodiments the analyte is charged.

Another aspect of the present invention is the use of a nanopore sensor as described above the detection of an analyte in a sample.

In specific embodiments the analyte is a small molecule, a protein, or a nucleic acid.

In specific embodiments, the analyte is charged.

BRIEF DESCRIPTION OF DRAWINGS

Figure 1 shows internalization of AlkB-Fe^{++} into ClyA-AS. Fig. 1a shows a cartoon representation of *E. coli* AlkB (green) containing a metal ion (Co^{2+}, sphere) and binding to the cofactor (2-OG, labeled). The DNA binding site is depicted by an orange line. PDB_ID 3KHB. Fig. 1b shows the representation of a single AlkB-Fe^{++} enzyme confined in a ClyA-AS nanopore (shown as cross-section) embedded in a planar lipid bilayer (labeled) under a negative applied potential. The dimensions of the pore consider the Van der Waals radii of the atoms. Fig. 1c, (top panel) shows typical current blockades provoked by AlkB-Fe^{++} molecules (~4 nM, *cis*) entering a ClyA-AS nanopore at -60 mV. The open pore current (I_O) is represented by a blue dashed line, while Level 1 and Level 2 are shown by dashed lines, respectively. The asterisks represent the restoration of I_O upon the exiting of AlkB-Fe^{++} from the pore. The bottom panel shows the detail of a single AlkB-Fe^{++} blockade, showing Level 1 and Level 2 current levels. The current traces were collected by applying a Bessel-low pass filter with a 2 kHz cut-off and sampled at 10 kHz. An additional Bessel 8-pole filter with 50 Hz cut-off was digitally applied to the traces shown in Fig. 1c (bottom

panel). All recordings were carried out in 150 mM NaCl, 15 mM Tris HCl pH 8.0, at 28°C, and the AlkB was added to the *cis* compartment.

Figure 2 shows binding of ligands to AlkB-Fe^{++} confined inside ClyA-AS. Fig. 2a shows a typical ligand-induced blockades to individual AlkB-Fe^{++} enzymes confined inside ClyA-AS at -60 mV. The ligand used is shown on the right of the trace. The bound Level 1 current levels (L_{1O}, L_{1N}, L_{1S}) are represented by the lowermost dashed lines. The substrate concentration was 0.6 mM for 2-OG, 0.6 mM for N-OG and 2 mM for SUC binding to wild type AlkB-Fe^{++}, and 7.2 mM for 2-OG binding to N120D-AlkB-Fe^{++}. Fig. 1b (left panel) shows dissociation rate constants (k_{off}) as a function of the ligand concentration at -60 mV; while Fig. 1b (right panel) shows Event frequency ($1/\tau_{on}$) as a function of the ligand concentration at -60 mV. 2-OG is shown in squares, SUC in circles and N-OG in triangles. All values for k_{off} and f are based on >350 binding events in total collected from N>3 single channel experiments with each experiment typically analysing n>8 AlkB blockades. All current traces were collected by applying a Bessel-low pass filter with a 2 kHz cut-off and sampled at 10 kHz. An additional Bessel 8-pole filter with 50 Hz cut-off was digitally applied to the current traces. All recordings were carried out in 150 mM NaCl, 15 mM Tris HCl pH 8.0, at 28°C, and the ligands were added to the *cis* compartment. Errors are given as standard deviations.

Figure 3 shows DHFR as a protein adaptor. Fig. 3a is a cartoon representation of *E. coli* DHFR (labeled) with bound methotrexate (MTX, spheres) and NADPH (spheres), PDB_ID 1RH3. Fig. 3b shows a representation of a single $DHFR_{tag}$ enzyme in complex with MTX confined in a ClyA-AS nanopore (shown as cross-section) embedded in a planar lipid bilayer (labeled) under a negative applied potential. The positively charged polypeptide tag added at the C-terminus of DHFR is labeled. Fig. 3c shows typical current blockades provoked by the capture of $DHFR_{tag}$:MTX complexes (20 nM $DHFR_{tag}$, 400 nM MTX, *cis*) by the ClyA-AS nanopore at -90 mV. The open pore current (I_O) is represented by the lowermostdashed line, while L_{1M} and L_{2M} are shown by the middle and uppermost dashed lines, respectively. Asterisks represent restoration of I_O upon the exiting of $DHFR_{tag}$:MTX from the pore. The current traces were collected in 150 mM NaCl, 15 mM Tris HCl pH 7.5, at 28°C by applying a Bessel-low pass filter with a 2 kHz cut-off and sampled at 10 kHz.

Figure 4 shows current enhancements upon ligand binding to $DHFR_{tag}$ Fig. 4a shows ligand-induced current enhancements to individual $DHFR_{tag}$:MTX blockades at -90 mV. NADP+ and NADPH were added to the *trans* compartment after addition of 20 nM $DHFR_{tag}$ and 400 nM MTX to the *cis* compartment. From top to bottom: no ligand; 5.7 µM of NADP+; 0.7 µM of NADPH; 7.4 µM of NADP+ together with 0.7 µM of

NADPH. Free and bound Level 1 (L1 and L1o) are shown by dashed lines. Asterisks represent restoration of I_O upon the exit of $DHFR_{tag}$:MTX from the pore. On the right of the current traces is the schematic representation of the interaction of $DHFR_{tag}$ with MTX, NADP+ or NADPH. Fig. 4b (top panel) shows dissociation rate constants (k_{off}) as a function of the NADP+ concentration added to the *trans* compartment at -90 mV. Fig. 4b (bottom panel) shows event frequency ($1/\tau_{on}$) as a function of the NADP+ concentration added to the *trans* compartment at -90 mV. Errors are shown as standard deviations. All values for k_{off} and f are based on > 2000 binding events in total collected from N> 8 single channel experiments with each experiment typically analysing n> 20 $DHFR_{tag}$:MTX blockades. All current traces were collected by applying a Bessel-low pass filter with a 2 kHz cut-off and sampled at 10 kHz. An additional Bessel 8-pole filter with 50 Hz cut-off was digitally applied to the traces shown in Fig. 4a. All recordings were carried out in 150 mM NaCl, 15 mM Tris HCl pH 7.5, at 28°C.

Figure 5 shows 2-OG induced binding events to a single AlkB-Fe^{++} molecule. The current trace shows the capture of an AlkB-Fe^{++} molecule (arrow) previously added to the *cis* compartment followed by the addition of 2-OG to the *cis* compartment. Confined AlkB-Fe^{++} showed L1 and L2 current levels, while 2-OG binding induced L1B and L2B ionic current levels. (All current levels are labeled). The grey dashed line corresponds to the open pore current (I_o). The trace was recorded at -60 mV applied potential in 150 mM NaCl, 15 mM Tris.HCl pH 8.0 at 28°C using 2 kHz filtering and 10 kHz sampling rate, and filtered digitally with a Bessel (8-pole) low-pass filter with 50 Hz cut-off.

Figure 6 shows 2-OG induced current levels to AlkB-Fe^{++}. Fig. 6a shows an extended current trace showing L1, L1B, L2 and L2B current levels induced by the binding of 2-OG to a single confined AlkB-Fe^{++}. In Fig. 6b are selected traces showing the details of the ligand-induced current levels. Transitions were always from L1B to L2B or from L1 to L2, or from L2 to L1 or from L2B to L1B. Current traces were recorded in presence of 4.8 mM 2-OG at -60 mV applied potential in 150 mM NaCl, 15 mM Tris.HCl pH 8.0 at 28°C using 2 kHz filtering and 10 kHz sampling rate, and filtered digitally with a Bessel (8-pole) low-pass filter with 50 Hz cut-off.

Figure 7 shows NADP+ induced binding events to $DHFR_{tag}$:MTX. The current trace shows $DHFR_{tag}$:MTX (added to the *cis* compartment, 50 nM of $DHFR_{tag}$ and 400 nM MTX) blockades before (left) and after (right) the addition of 5.7 µM NADP+ (arrow) to the *trans* compartment. The binding of NADP+ results in reversible current enhancements from $L1_M$ (uppermost dashed line) to $L1_{M:N+}$ (labeled). The grey dashed line (lowermost dashed line) corresponds to the open pore current (I_o). The trace was recorded at -90 mV applied potential in 150 mM NaCl, 15 mM Tris.HCl pH

7.5 at 28°C using 2 kHz filtering and 10 kHz sampling rate, and filtered digitally with a Bessel (8-pole) low-pass filter with 50 Hz cut-off.

Figure 8 shows the effect of the cognate Anti-AlkB aptamer on the AlkB-Fe^{++}-induced current blockades. The addition of 40 µM cognate aptamer (TGCCTAGCGTTTCATTGTCCCTTCTTATTAGGTGATAATA, SEQ ID NO: 27, Table 5) reduced the frequency of the AlkB-Fe^{++} blockades to ClyA-AS caused by 21 nM AlkB_Fe^{++} due to electrostatic repulsion and/or steric hindrance between the AlkB:aptamer complexes and the negatively charged ClyA-AS lumen (Soskine, M. (2012) *Nano Lett.* **12**, 4895-4900). The recordings were carried out in 150 mM NaCl, 15 mM Tris HCl pH 8.0 at 28°C and -35 mV applied potential.

Figure 9 shows heterogeneity of NADPH and NADP+ binding to $DHFR_{tag}$:MTX. In Figs. 9a and 9b, the current traces show the capture of $DHFR_{tag}$:MTX inside ClyA-AS (50 nM of $DHFR_{tag}$ and 400 nM of MTX added to the *cis* compartment), after the addition of 0.74 µM NADPH to the *trans* compartment. The uppermost dashed line represents the $DHFR_{tag}$:MTX $L1_M$ level. The asterisks indicate "short" (*i.e.* low affinity) NADPH binding events, while the solid lines indicate "long" (*i.e.* high affinity) NADPH induced binding events. The arrows show the capture of a new $DHFR_{tag}$:MTX complex. The current trace in (a) shows $DHFR_{tag}$:MTX blockades displaying either "short" or "long" NADPH binding events. The current trace in (b) shows the switching between "short" and "long" binding modes within the same $DHFR_{tag}$:MTX blockade. Figs. 9c and 9d show $DHFR_{tag}$:MTX blockades (50 nM $DHFR_{tag}$ and 400 nM MTX in *cis*) after the addition of 5.7 µM NADP+ in *trans*. The dashed line represents the $DHFR_{tag}$:MTX $L1_M$ level, the non-responsive state of the binary complex towards NADP+ is indicated by a solid line. The arrows indicate the capture of a new $DHFR_{tag}$:MTX complex. The current trace in (c) shows $DHFR_{tag}$:MTX blockades that are either responsive or non-responsive towards NADP+ addition. The current trace in (d) shows the switching between non-responsive and responsive states within the same $DHFR_{tag}$:MTX blockade. The traces were recorded at -90 mV applied potential in 150 mM NaCl, 15 mM Tris.HCl pH 7.5 at 28°C using 2 kHz filtering and 10 kHz sampling rate, and filtered digitally with a Bessel (8-pole) low-pass filter with 50 Hz cut-off.

Figure 10 shows sequences of the 1+, 4+, tag (5 positive charges) and 10+ fusions to the DHFR C-terminus. The C-terminus of DHFR, the sequences of the S-tag, the positive coil and the Strep-tag are colored green, gray, cyan and yellow, respectively. The sequences of the flexible linkers are underlined. The positively charged amino acids in the polypeptide tags are indicated by an asterisk (*) and the negatively charged amino acids by a minus sign (-).

Figure 11 show $DHFR_{n+}$, $DHFR_{n+}$:MTX and $DHFR_{n+}$:MTX:NADPH induced current blockades to ClyA-AS nanopores. Representative traces recorded in presence of ~ 50 nM of Fig. 11a: DHFR, Fig. 11b: $DHFR_{10+}$, Fig. 11c: $DHFR_{4+}$, Fig. 11d: $DHFR_{tag}$ added to the *cis* compartment. Every set of three panels shows $DHFR_{n+}$ blockades recorded without ligands (left panel), after the addition of 400 nM MTX to the *cis* compartment (centre panel) and after further addition of 20 μM of NADPH in *cis* (a) or 0.7 μM of NADPH to the *trans* compartment (Figs. 11b, 11c, 11d) (right panel). The arrows indicate NADPH binding events to the binary $DHFR_{n+}$:MTX complexes. The asterisks indicate the transition of $DHFR_{10+}$:MTX to a lower conductance level. Current traces were recorded at -90 mV applied potential in 150 mM NaCl, 15 mM Tris.HCl pH 7.5 at 28°C using 2 kHz filtering and 10 kHz sampling rate, and filtered digitally with a Gaussian low-pass filter with 500 Hz cut-off.

Figure 12 shows the purity of the strep-tagged purified wild type AlkB-Fe^{++} assayed by a 12 % SDS PAGE. In the left lane is a protein marker (Page Ruler Plus Prestained Protein Ladder, Thermo scientific); in the right lane is 5 μg of the purified AlkB-Fe^{++}.

Figure 13 shows the purity of the strep-tagged purified $DHFR_{n+}$ assayed by a 15 % SDS PAGE. In lane 1 is a protein marker (Page Ruler Plus Prestained Protein Ladder, Thermo scientific). Lanes 2-4 contain ~ 5 μg each of purified DHFR (lane 2), $DHFR_{4+}$ (lane 3), $DHFR_{tag}$ (lane 4) and lane 5 contains ~ 10 μg of purified $DHFR_{10+}$.

Figure 14 SBD (substrate-binding domains) proteins with the ClyA nanopore.
Left. Type I ClyA-AS nanopore embedded in the lipid bilayer. The dimensions of the ClyA nanopores are indicated considering the van der Waals radii of the atoms. Right. Upper part, surface representation of SBD1 in the open configuration (PDB ID = 4LA9). Lower part, surface representation of SBD2 in the open (PDB ID = 4KR5) and closed, Gln-bound (PDB ID = 4KQP) configuration. The proteins are colored according to their "in vacuum" electrostatics (red for negative regions and blue for positive regions, Pymol).

Figure 15 shows the capture of SBD1 in Type I ClyA-AS
(A) Typical ionic current blockades provoked by the capture of SBD1 (substrate-binding domain 1) (74 nM, *cis*) by the type I ClyA-AS nanopore at -60 mV. The open pore, Level I and Level II current levels are indicated. (B) Detail of SBD1 current blockade before (upper part) and after addition of 0.40 μM asparagine (*cis*). The current traces were collected in 150 mM NaCl, 15 mM Tris-HCl, pH 7.5 at 24°C by applying a Bessel low-pass filter with a 2 kHz cutoff and sampled at 10 kHz. A post-acquisition Gaussian filter of 100 Hz was applied. (C) K_d values of SBD1 (74 nM, *cis*) for asparagine, obtained from the open (Level I) and closed ligand-bound (Level II) populations at the indicated substrate concentrations. Experiments were performed

at -60 mV. (D) Opening ($k_{opening}$) and closing ($k_{closing}$) rate constants of SBD1 determined from the transition rates of SBD1 molecules trapped in the nanopore at -60 mV as a function of asparagine concentration. The $k_{closing}$ was obtained from the slope of the linear fit.

Figure 16 shows capture of SBD2.

(A) Typical current blockade provoked by the capture of SBD2 (70 nM, *cis*) by the type I ClyA-AS nanopore at -100 mV before (left) and after addition of 0.40 µM glutamine *cis*. The current traces were collected in 150 mM NaCl, 15 mM Tris-HCl, pH 7.5 at 24°C by applying a Bessel low-pass filter with a 2 kHz cutoff and sampled at 10 kHz. A post-aqcuisition Gaussian filter of 100 Hz was applied. (B) K_d values of SBD2 (70 nM, *cis*) for glutamine, obtained from Level II (bound state), and level I and Level III at the indicated substrate concentrations. Experiments were performed at -100 mV. (C) Opening ($k_{opening}$) and closing ($k_{closing}$) rate constants of SBD2.

Figure 17 shows that inactive SBD2 does not bind to glutamine.

(A) Typical current blockade provoked by the capture of E417W-SBD2 (*cis*) by the type I ClyA-AS nanopore at -100 mV before (left) and after addition of 200 µM glutamine *cis*. Red asteriks represent the restoration of I_o upon the exiting of SBD2_D417F from the pore. Level I and Level II transition most likely represent the entry of SBD2 into ClyA nanopores in two different configurations.

Figure 18. Glucose sensing with a venus flytrap protein domain. a) Cut-through a ClyA nanopore containing a GBP. b) Cartoon representation of the open (blue) and closed (orange) configuration of the venus flytrap domain of GBP. c) Electrical recording of the GPB blocked current in the absence (top) and presence (middle and bottom) of increasing concentrations of glucose.

Figure 19 shows protein recognition with ClyA variants.

A) Cut through a ClyA-AS nanopore showing the incorporation of HT. The protein lodges in two sites inside the nanopore which are called L1 and L2. B) Ionic current blockades of HT inside ClyA-AS showing the movement of HT between L1 and L2 at -35 mV. C) Percentage of L1 and L2 residence inside ClyA-AS for different ClyA-AS mutants.

Figure 20 Shows the effect of nanopore mutations on Human thrombin blockades. The figure indicate the blockades induced by human thrombin at -35, -50 and -80 mV (from top to bottom) to ClyA-AS-WT, CLyA-AS-125W and ClyA-AS-v60w (from left to right). THe blockades induced by human thrombin are similar for ClyA-AS-WT and CLyA-AS-125W, and differ for ClyA-AS-v60w, indicating that thrombin binding site is close to the position 60 inside the ClyA nanopore.

Figure 21 shows analyte recognition with ClyA nanopores.

A) Binding of Glutamine to SBD2 inside a ClyA-AS nanopore. Level I and Level III correspond to the open SBD2 configuration (see word file), while Level II corresponds to the ligand bound configuration.

B) mutant screened showing the difference between level I, Level II and Level III (as residual current %). Q56W provides the better recognition.

Figure 22 shows SBD2 blockades to ClyA-AS-q56w. The signal due to the binding of glutamine to the internalized adaptor (level L2)is enhanced when compared to the signal measured for the ClyA-WT pore (Figure 21)

DETAILED DESCRIPTION OF INVENTION

Proteins have evolved to identify their ligands with high specificity in a sea of very similar chemical species. Accordingly, a nanopore which has incorporated protein adaptors in the lumen of the nanopore is well-suited for use in detecting ligand analytes. When the internalized protein adaptor binds to its target analyte, the conformational change in the protein adaptor and/or presence of the target analyte bound to the protein adaptor is measured as a change in nanopore conductance, for example, as an increase in the ionic current blockade events in the nanopore.

Accordingly, one aspect of the present disclosure relates to nanopore sensors comprising a nanopore (also called “pore,” “pore protein,” or “nanopore protein”)and a protein adaptor (or “adaptor” or “internalized protein” or “protein”) which is fully or partially internalized (or “contained,” “incorporated,” “trapped,” “set,” “accomodated,” “residing,” “embedded,” or “confined”) within the lumen of the nanopore.

Nanopores

Exemplary nanopores include, but are not limited to cytolysins, hemolysins, porins, DNA packaging protein, and motor proteins. In some embodiments, the nanopore is Phi29 (Wendell, D. et al. (2009) *Nat. nanotech.* **4**, 765-772), pneumolysin (Gilbert, R. J. et al. (1999) *Cell* **97**, 647-655), FhuA (Niedzwiecki DJ et al. (2012) Biophys J. **103,** 2115-2124) or a solid-state nanopores.

In certain embodiments, the nanopore is a pore-forming cytotoxic protein, for example, a bacterial cytolysin. In certain embodiments, the nanopore is a cytolysin from a gram-negative bacteria such as *Salmonella* or *Escherichia coli* (*E. coli*). In some embodiments, the nanopore is Cytolysin A (ClyA) from *Salmonella typhi* (*S. typhi*) or *Salmonella paratyphi* (*S. paratyphi*). In some embodiments, the nanopore is a mutant or variant of ClyA, such as a modified variant of ClyA like ClyA-CS or ClyA-AS as described in WO2014153625.

In certain embodiments, the nanopore is cylindrically shaped with at least 2 openings, for example, a cis opening and a trans opening. A first opening may have a larger diameter than a second opening in the nanopore. In some embodiments, the *cis* opening has a larger diameter than the *trans* opening. Thus, the "*cis* diameter" is wider than the "*trans* diameter." Alternatively, the *trans* opening may have a larger diameter than the *cis* opening. Typically, a nanopore is an oligomeric structure comprising subunits (or "monomers"), and the size of the pore lumen depends on the number and/or composition of subunits in the oligomeric structure. In some embodiments, the nanopore may comprise at least 7 monomers, for example, 7, 8, 9, 10, 11, 12, 13, 14, 15, 16, 17, 18, 19, or 20 monomer subunits. In some embodiments, the nanopore comprises at least 20 monomer subunits, for example, 20-25, 25-30, 35-40, or 45-50 subunits. In certain embodiments, the nanopore comprises 12 subunits. In further embodiments, the nanopore comprises 13 subunits, or 14 subunits. The subunits may preferentially assemble in 12mers and/or 13mers, depending on the amino acid sequence of the subunits.

The nanopores comprise subunits which may be assembled into different oligomeric forms. Within a single nanopore (for example a ClyA nanopore), each of the subunits may be identical, or the subunits may be different, so that subunits in a pore may comprise sequences that differ from sequences of other polypeptide subunits in the same nanopore. In certain embodiments, nanopores as disclosed herein, such as ClyA nanopores or variants such as ClyA-CS and ClyA-AS, may form more than one subtype depending on subunit composition. For example, there may be at least 2 or 3 different subtypes of subunits in the nanopore, depending on the composition of the subunits. ClyA-AS [Mueller, M. et al. (2009) *Nature*, **459**, 726-730; Soskine, M. et al. (2013) *J Am Chem Soc*, **135**, 13456-13463] (SEQ ID NO:3) may be assembled into at least 3 oligomeric forms (Type I, Type II and Type III ClyA) (Soskine, M. et al. (2013) *J Am Chem Soc*, **135**, 13456-13463) that are large enough to accommodate proteins or protein-DNA complexes (Van Meervelt, V. et al (2014) *ACS nano*, **8,** 128262-12835). Any nanopore that is assembled from individual subunits may have different oligomeric forms, and the oligomeric forms may vary in properties such as size and voltage dependent opening and closing (gating) of the nanopore. Subtypes may be preferentially formed by subunits of a particular polypeptide sequence.

In some embodiments, the nanopore is ClyA from *Salmonella typhi* and comprises a plurality of subunits, wherein each subunit comprises a polypeptide represented by an amino acid sequence at least 80% identical to SEQ ID NO: 1. In certain embodiments, the subunits are represented by an amino acid sequence at least 85%

identical, 90% identical, 95% identical, 99% identical or 100% identical to SEQ ID NO:1. Identical may refer to amino acid identity, or may refer to structural and/or functional identity. Accordingly, one or more amino acids may be substituted, deleted, and/or added, as compared with SEQ ID NO:1. Modifications may alter the pore lumen in order to alter the size, binding properties, and/or structure of the pore. Modifications may also alter the ClyA nanopore outside of the lumen.

In certain embodiments, the ClyA nanopore comprises a plurality of subunits, wherein each subunit comprises a polypeptide represented by an amino acid sequence of SEQ ID NO:1 (or a sequence that is at least 85%, 90%, 95%, 96%, 96%, 98%, or 99% identical to SEQ ID NO:1), and wherein exactly one Cys residue is substituted with Ser. The Cys residue may be Cys 87 and/or Cys 285 in SEQ ID NO:1. In some embodiments, the Cys residue is Cys285. The remaining amino acid residues may also be substituted, for example, with amino acids that share similar properties such as structure, charge, hydrophobicity, or hydrophilicity. In certain embodiments, substituted residues are one or more of L99, E103, F166, and K294. For example, the substituted residues may be one or more of L99Q, E103G, F166Y, and K294R. An exemplary subunit may comprise substitutions L99Q, E103G, F166Y, K294R, and C285S. Thus, each subunit may comprise a polypeptide represented by an amino acid sequence of SEQ ID NO:2. An exemplary ClyA nanopore comprising subunits in which exactly one Cys residue is substituted with Ser may be called ClyA-CS.

Other ClyA mutants of the present invention are variants with a mutation at Ser110, Lys125, Val67, Val60, Gln56 or Arg49. Specific embodiments of such variants are Lys125Trp, Val60Trp and Gln56Trp.

In some embodiments, the ClyA nanopore comprises a plurality of subunits, wherein each subunit comprises a polypeptide represented by an amino acid sequence of SEQ ID NO:1 (or a sequence that is at least 85%, 90%, 95%, 96%, 96%, 98%, or 99% identical to SEQ ID NO:1), and wherein exactly one Cys residue is substituted with Ala. The cysteine residue may be Cys 87 or Cys 285 in SEQ ID NO:1. In some embodiments, each subunit comprises a polypeptide represented by an amino acid sequence of SEQ ID NO:1 (or a sequence that is at least 85%, 90%, 95%, 96%, 96%, 98%, or 99% identical to SEQ ID NO:1), wherein one Cys residue is substituted with Ser and/or exactly one Cys residue is subsituted with Ala. The cysteine residues may be Cys87 or Cys285 in SEQ ID NO:1. Other amino acid residues may be substituted, for example, with amino acids that share similar properties such as structure, charge, hydrophobicity, or hydrophilicity. In certain embodiments, substituted residues are one or more of L99, E103, F166, K294, L203 and H207. For example, the substituted residues may be L99Q, E103G, F166Y, K294R, L203V, and

H207Y. An exemplary subunit may comprise L99Q, E103G, F166Y, K294R, L203V, and H207Y, and C285S. Accordingly, each subunit may comprise a polypeptide represented by an amino acid sequence of SEQ ID NO:3. An exemplary ClyA nanopore comprising subunits in which exactly one Cys residue is substituted with Ser and exactly one Cys residue is substituted with Ala may be called ClyA-AS.

The present disclosure further relates to nucleic acids encoding the modified ClyA nanopores. In some embodiments, a nucleic acid encoding a modified ClyA nanopore is represented by a nucleotide sequence that is at least 80%, 90%, 95%, 96%, 96%, 98%, or 99% identical to SEQ ID NO:4. A nucleic acid may be represented by SEQ ID NO: 5 or SEQ ID NO:6. Nucleotide sequences may be codon optimized for expression in suitable hosts, for example, *E. coli*.

In some embodiments, the lumen of the nanopore is large enough to accommodate a protein adaptor that is folded and is either (1) not bound or (2) bound to a target such as a specific target analyte. The protein adaptor may be complexed with one or more additional molecules such as a co-factor or substrate or inhibitor to form a protein adaptor complex (or "adaptor complex"). The protein adaptor may bind non-specifically and/or with low affinity to non-targets before binding with high affinity to its target, particularly if the non-targets are chemically similar to the target. In heterogeneous biological samples, the protein adaptor may be exposed to a variety of analytes that are not its target analyte. The protein adaptor may also undergo conformational changes within the lumen of the nanopore upon binding to its target analyte.

In certain embodiments, the lumen of the nanopore is at least 3 nm in diameter, for example, the diameter may measure 3 nm, 3.5 nm, 4 nm, 4.5 nm, 5 nm, 5.5 nm, 6 nm, 6.5 nm, 7 nm, or greater. The *cis* diameter of the nanopore lumen may be at least 3.5 nm and/or the *trans* diameter of the nanopore may be at least 6 nm. In general, *cis* refers to the end of the modified pore to which an analyte is added, while *trans* refers to the end of the modified nanopore through which the analyte exits after translocating the length of the nanopore lumen. In artificial lipid bilayers, for example, the *trans* end of a pore may be inserted in the lipid bilayer, while the *cis* end of the nanopore remains on the same side of the lipid bilayer. Accordingly, the *cis* diameter of the nanopore is the diameter of the opening at the *cis* end of the nanopore, while the *trans* diameter of the nanopore is the diameter at the opening of theopposite *trans* end of the nanopore. An analyte may be added to either side of the nanopore, for example, an analyte may be added to the the *cis* opening of the nanopore so that it transverses the nanopore and exits from the *trans* side. Alternatively, an analyte may be added to the *trans* side of the nanopore. Nanopores

are typically arrayed in a membrane such as a lipid bilayer, across which a potential can be applied. In general, the applied potential across the membrane refers to the potential of the *trans* electrode. Nanopores may be inserted into lipid bilayers from the *cis* compartment, which are connected to a ground electrode.

Protein Adaptors

A variety of protein adaptors may be fully or partially incorported in the lumen of nanopores to form the nanopore sensors. In some embodiments, the protein adaptors are globular proteins (also called "spheroproteins"). The protein adaptors may be roughly spherical and may form colloids in water. For example, the protein adaptors may be characterized by apolar (hydrophobic) amino acids that are bounded towards the molecule's interior while polar (hydrophilic) amino acids are bound outwards.

In some embodiments, the protein adaptor is a single protein. In certain embodiments, the protein adaptor is a protein domains, oligomers, and/or fragment of a protein. The protein adaptor may also be a complex or combination of single proteins and/or fragments. In certain embodiments, the protein adaptor complex comprises a protein (or fragments or domains) complexed with a small analyte such as a small molecule and/or an inhibitor. In certain embodiments, the protein adaptor is a functional enzyme. In certain embodiments, the protein adaptor is a ligand-binding domain.

The protein adaptor must have dimensions that fit into a nanopore, for example, the protein adaptor may have a diameter that is smaller than the *cis*-diameter of the nanopore but larger than the *trans*-diameter of the nanopore. In some exemplary nanopores, the cis-diameter is wider than the trans-diameter, so the protein adaptor may pass through the cis end of the nanopore but not through the trans end. The protein adaptor may remain internalized for at least 0.1-1 μs, 1-10 μs, or 10-100 μs. The *cis*-diameter of the nanopore may be at least 4.5 nm, 5.0 nm, 5.5 nm, 6.0 nm, 6.5 nm, or 7 nm, while the *trans*-diameter of the nanopore is at least 1.5 nm, 2.0 nm, 3.0 nm, 3.3 nm, 3.5 nm, or 4.0 nm. In certain embodiments, the *cis*-diameter of the nanopore is 5.5 nm and the *trans*-diameter of the nanopore is about 3.0 nm, for example 3.3 nm. A protein adaptor suitable for internalization in the nanopore may have an average diameter that is smaller than the cis-diameter of the nanopore (for example, smaller than 5.5 nm) but larger than the trans-diameter of the nanopore (for example, larger than 3.0 nm or 3.3 nm). Accordingly, such a protein adaptor added to the *cis* side of the nanopore would be able to enter the nanopore but would not exit from the *trans* side of the nanopore. Conversely, if the *trans*-

diameter were larger than the *cis*-diameter, then a protein adaptor added to the *trans* side of the nanopore would enter through the *trans*-opening but would not exit from the *cis*-opening.

The average diameter of the protein adaptor may be determined by examination of the crystal structure, if available, or by estimation based on measurements such as molecular weight. For example, a protein with a molecular weight of about 20 kDa may be expected to have an average diameter of less than 3.5 nm, while a protein with a molecular weight of about 25 kDa may be expected to have an average diameter of more than 3.5 nm.

Nanopores typically have lumens that are either negatively or positively charged, as the charge is required for the electroosmotic flow of charged molecules (e.g., analytes) through the nanopore when an electric field is applied across the nanopore. For example, when a nanopore has a negatively-charged lumen and a negative potential is applied to one side of the nanopore (e.g., the trans side of the nanopore), then a positively charged molecule will pass freely through the nanopore from the cis end to the trans end. Accordingly, for nanopores with negatively-charged lumen, protein adaptors suitable for internalization in the nanopore may be positively- or negatively- charged. Charges are not limiting for the incorporation of the protein adaptor. For example, moderately negatively-charged molecules (pI>4 –isoelectric point) can be incorporated.

Some protein adaptors are either too small to remain internalized in the nanopore and/or have a charge is not suitable for entry into the nanopore (i.e., a nanopore has a negatively-charged lumen but the protein has a highly negative charge). For example, if a protein has an average diameter that is smaller than both diameters of the nanopore, the protein may not be expected to remain internalized in the nanopore lumen. A protein that has an average diameter of less than 3.5 nm would not be expected to remain internalized for longer than a few milliseconds in a nanopore whose *cis* diameter is about 6.5 nm and whose *trans* diameter is about 3.5 nm. In some embodiments, a protein adaptor is tagged in order to be internalized in the nanopore and/or to be retained in the lumen of the nanopore. The tag may be a charged tag. For example, a protein may have a positively-charged tag in order to be internalized in a negatively-charged nanopore. The tag may be attached covalently or by other chemical means, or the tag may be present as a fusion with the protein adaptor, for example, the protein adaptor and tag may have been genetically encoded. In some embodiments, a tag comprises at least 4, 5, 6, 7, 8, 9, or 10 positively charged amino acid residues. Tags may comprise positively charged coils, spacers (e.g., flexible linkers), and/or labels for purification (e.g., strep tags). In

some embodiments, the presence of a tag increases the retention time of the tagged protein adaptor by 100-fold or 1000-fold. Accordingly, the tagged protein adaptor may remain internalized in the nanopore for seconds whereas the untagged protein adaptor alone would only be internalized for milliseconds.

In some embodiments, the protein adaptor is an enzyme (also called an "enzyme adaptor"). The enzyme may be an oxidoreducase (Enzyme Commission (EC) 1), transferase (EC2), hydrolase (EC3), lyase (EC4), isomerase (EC5), or ligase (EC6). The enzyme may be selected from a demethylase or a reductase. In some embodiments, the enzyme is a demethylase. For example, the enzyme may be AlkB demethylase. In certain embodiments, the enzyme is a reductase, such as dihydrofolate reductase (DHFR). The protein adaptor may be complexed with a molecule such as a small molecule (e.g., co-factor, inhibitor, and/or any other small molecule that binds to the protein adaptor) to form an adaptor complex, and this adaptor complex may bind to a target analyte. For example, DHFR may be complexed with methotrexate (MTX) to form an adaptor complex.

In some embodiments, the protein adaptor comprises protein subunits, fragments, and/or domains of proteins. A protein subunit, fragment, or domain may be suitable for internalization, or may be made suitable by adding tags to increase size and/or charge. A protein adaptor complex may comprise a protein subunit, fragment, or domain.

Other exemplary protein adaptors include but are not limited to antibodies, nanobodies, artificially designed binding elements, ligand binding proteins (for example, venus fly trap domains), transcription factors, metal-binding proteins, intrinsically unfolded binders, and more.

Uses of Nanopore Sensors

(a) Detection and Identification of Analytes

Any analyte (or "target," "target analyte," "ligand," "substrate," or "binding partner") that binds to a protein adaptor may be detected using the nanopore sensors described herein. Analytes include small molecules, including organic and inorganic molecules, and biological molecules such as proteins and nucleic acids. Analytes may be charged or may be uncharged molecules. In some embodiments, the analytes detected by the nanopore sensors disclosed herein are charged molecules. The charged molecules may be proteins or small molecules.

Analytes may be known targets of the protein adaptor, for example, if the nanopore is used to determine whether a known binding partner of the protein adaptor is present in a mixture. Alternatively, new binding partners for the protein adaptor may

be identified, for example, by screening a library of compounds or molecules which were not previously known to bind to the protein adaptor.

Accordingly, one aspect of the present invention relates to a method for detecting an analyte in a sample, comprising obtaining a nanopore sensor comprising a nanopore and a protein adaptor internalized in the lumen of the nanopore, adding the sample to the *cis* side or the *trans* side of the nanopore, and measuring conductance across the nanopore, wherein a change in conductance after adding the sample indicates that the analyte is present in the sample and has bound to the protein adaptor. In some embodiments, conductance is measured continuously before, during, and after addition of the analyte.

A further aspect relates to a method for identifying a ligand for a protein adaptor, comprising obtaining a nanopore sensor comprising a nanopore and a protein adaptor internalized in the lumen of the nanopore, adding a test compound to the *cis* side or the *trans* side of the nanopore, and measuring the conductance across the nanopore, wherein a change in conductance after adding the test compound indicates that the test compound is a ligand that binds to the protein adaptor.

In some embodiments, the change in conductance is a change in the current blockades (I_B), i.e., residual currents calculated as a percentage of the open pore current (IRES%). Thus, binding of an analyte to the protein adaptor may cause an increase in current blockades. In some embodiments, the current blockade is decreased. In certain embodiments, the change in current conductance is a measurable change in the noise pattern.

Conductance across the nanopore is sensitive and highly specific to the identity of the ligand that binds to the protein adaptor. Conductance measurements may be used to differentiate between two ligands that differ from one another by a single atom. For example, the binding of a protein adaptor (or adaptor complex) to a specific substrate has a different conductance than the binding of the protein adaptor (or adaptor complex) to the substrate that lacks a hydride ion. Thus, binding of an internalized protein to NADPH may be distinguished from binding of the internalized protein to NADP+.

(b) Enzyme binding and activity

A protein adaptors may be an enzyme ("enzyme adaptor," "internalized enzyme," or "enzyme"), and various aspects of enzyme binding, activity, and function may be studied using a nanopore sensor comprising a nanopore and an enzyme adaptor. A further aspect of the present disclosure relates to a method for measuring enzyme kinetics, comprising obtaining a nanopore sensor comprising a nanopore and an

enzyme adaptor internalized in the lumen of the nanopore, adding a ligand to the *cis* side or the *trans* side of the nanopore, measuring a first conductance change across the nanopore which reflects binding of the ligand to the enzyme adaptor, and measuring additional conductance changes across the nanopore which reflect enzyme kinetics such as association and dissociation of the ligand and the enzyme adaptor. In some embodiments, the measurements are obtained continuously over time while the ligand concentration is varied (e.g., increased).

In certain embodiments, the method further comprises increasing the applied potential across the nanopore until the ligand dissociates from the enzyme adaptor, and the dissociation is measured by a change in conductance (for example, a decrease or increase in I_B). In certain embodiments, the method further comprises decreasing the applied potential across the nanopore until the ligand binds to the enzyme adaptor, and the binding is measured by a change in conductance (for example, an increase or decrease in I_B). In some embodiments, dissociation rate constants (k_{off}) is measured from the inverse of the dwell times of the ligand-binding events ($1/\tau_{off}$), and does not depend on the concentration of the ligand. In certain embodiments, the frequencies of the ligand-induced events ($f = 1/\tau_{on}$) increase linearly with the concentration of the ligand, from which slopes the association rate constants (k_{on}) are calculated.

Notably, the enzyme adaptor retains its structure, binding sites, and activity. The ligand of the enzyme adaptor may be a substrate for the enzyme. Thus, an additional aspect of the present disclosure relates to a method for measuring activity of an enzyme adaptor on a substrate, comprising obtaining a nanopore sensor comprising a nanopore and an enzyme adaptor internalized in the lumen of the nanopore, adding the substrate to the *cis* side or the *trans* side of the nanopore, and measuring conductance across the nanopore, wherein a change in conductance after adding the ligand indicates activity of the enzyme adaptor on the substrate. The activity may be binding, cleavage, conformational changes, and/or other changes mediated by enzymes acting on their substrate.

In some embodiments, competitive binding between two substrates can be monitored by conductance changes as the substrates bind and dissociate with the enzyme adaptor.

All publications and patents mentioned herein are hereby incorporated by reference in their entirety as if each individual publication or patent was specifically and individually indicated to be incorporated by reference. In case of conflict, the present application, including any definitions herein, will control.

While specific embodiments of the subject invention have been discussed, the above specification is illustrative and not restrictive. Many variations of the invention will become apparent to those skilled in the art upon review of this specification and the claims below. The full scope of the invention should be determined by reference to the claims, along with their full scope of equivalents, and the specification, along with such variations.

The invention is now illustrated with examples which disclose specific embodiments of the invention.

EXAMPLES

EXAMPLE 1 MATERIAL & METHODS

Unless otherwise specified all chemicals were bought from Sigma-Aldrich. DNA was purchased from Integrated DNA Technologies (IDT), enzymes from Fermentas and lipids from Avanti Polar Lipids. Stocks of NADPH and NADP+ (prepared in 15 mM Tris.HCl pH 7.5 150 mM NaCl) were kept at -20 ºC and defrosted for single use. All errors in this work are given as standard deviations. The standard deviations (SD) for the values calculated from linear fits (Fig. 1e, Fig. 2e) were calculated from standard errors (SE) given by the fit by applying the formula $SE = \frac{SD}{\sqrt{N}}$ where N is the number of independent data points in the graph.

AlkB cloning

To allow cloning, a Nco I site (CCATGG) was introduced in the wild type AlkB from *E. coli* at the beginning of the gene (5' end). To keep the gene in reading frame an additional two bases were inserted after the Nco I site, resulting in an additional alanine residue after the starting methionine. For purification purposes, at the C-terminus of AlkB, a strep-tag was attached via a flexible glycine-serine-alanine linker and the open reading frame was terminated by two consecutive stop codons, followed by a Hind III restriction site (3' end). The attachment of the strep-tag was carried out in two consecutive PCR reactions. During the first PCR reaction, the AlkB gene was amplified directly from the genomic DNA of a single BL21(DE3) *E. coli* (Lucigen) colony using Phire Hot Start II DNA polymerase (Finnzymes), 6 μM fAlkB (Table 5) and AlkBr1 (Table 5) primers in a 50 μL reaction volume. The PCR reaction cycling protocol was as follows: pre-incubation step at 98ºC for 30 s and then 30 cycles of denaturation at 98ºC for 5 s and extension at 72ºC for 1 min. The amplified product was purified using QIAquick PCR Purification Kit (Qiagen) and served as a template for the second PCR reaction, which used ~100 ng of the purified PCR product

amplified by Phire Hot Start II DNA polymerase using 6 μM of fAlkB (Table 5) and AlkBr2 (Table 5) primers in 300 μL volume. The cycling protocol was the same as in the previous step. The resulting PCR product containing the strep-tagged AlkB gene was purified with QIAquick PCR Purification Kit (Qiagen) and digested with Nco I and Hind III (FastDigest, Fermentas). The gel purified insert (QIAquick Gel Extraction Kit, Qiagen) was cloned under control of the T7 promoter into the pT7-SC1 expression plasmid using sticky-end ligation (T4 ligase, Fermentas) via Nco I (5') and Hind III (3') sites. 0.6 μL of the ligation mixture was transformed into 50 μL of E. cloni® 10G cells (Lucigen) by electroporation. The transformed bacteria were grown overnight at 37ºC on ampicillin (100 μg/ml) LB agar plates. The identity of the clones was confirmed by sequencing. The DNA and proteins sequences of strep-tagged AlkB are included in the sequence listing (see Table 6).

Construction of the $DHFR_{n+}$ genes

The synthetic gene encoding for *E. coli* DHFR was made by GenScript. The wild-type gene was modified by the substitution of the two Cys residues at positions 85 and 152 with Ala and Ser respectively (referred to as DHFR throughout SI and main text). Those substitutions were shown to be functionally tolerated by DHFR (Plesa, C. et al. (2013) *Nano Lett.*, **13**, 658-663). Further, the DNA sequence encoding for Met-Ala-Ser-Ala was added at the beginning of the gene in order to introduce a Nco I restriction site. To facilitate construction steps, a Xho I restriction site was introduced between the C-terminal tags and DHFR.

As a first step the $DHFR_{10+}$ construct was built (Fig. 10, for DNA and protein sequence see below). 100 ng of the synthetic DHFR gene was amplified with 5 μM of DHf and DHr primers (Table 5) with Phire Hot Start II DNA polymerase (Finnzymes) in 400 μL final volume (pre-incubation at 98ºC for 30s, then cycling: denaturation at 98ºC for 5 s, extension at 72ºC for 1 min for 30 cycles). The synthetic fragment encoding for the 10+ tag (made by IDT, for sequence see below) was amplified as described above using Cof and Cor primers (Table 5). DHf and Cof primers contain sequences that are the reverse-complement of each other, introducing sequence overlap between DHFR and 10+ tag PCR products, necessary for the next step, where both PCR products (2 μg each, gel-purified, QIAquick Gel Extraction Kit, Qiagen) were assembled together using Phire Hot Start II DNA polymerase (Finnzymes) in 50 μL final volume (pre-incubation at 98ºC for 30s, then cycling: denaturation at 98ºC for 5 s, extension at 72ºC for 1 min for 7 cycles). ~100 ng of the purified (QIAquick PCR Purification Kit (Qiagen)) assembly product was amplified with 5 μM of DHf and Cor primers (Table 5), using Phire Hot Start II DNA polymerase (Finnzymes) in 400 μL final volume (pre-incubation at 98ºC for 30s, then cycling: denaturation at 98ºC for 5 s, extension at

72ºC for 1 min for 30 cycles). PCR product encoding for the whole length $DHFR_{10+}$ was purified using the QIAquick PCR Purification Kit (Qiagen) and digested with Nco I and Hind III (FastDigest, Fermentas). The resulting insert was gel purified and cloned under control of the T7 promoter into the pT7-SC1 expression plasmid [Miles, G. et al. (2001) *Biochem.* **40**, 8514-8522] using sticky-end ligation (T4 ligase, Fermentas) via Nco I (5') and Hind III (3') sites. 0.6 µL of the ligation mixture was transformed into E. cloni® 10G cells (Lucigen) by electroporation. The transformed bacteria were selected overnight at 37ºC on ampicillin (100 µg/ml) LB agar plates. The identity of the clones was confirmed by sequencing. The DNA and protein sequence of $DHFR_{10+}$ is provided below with the 10+ tag sequence indicated by capital letters in the DNA sequence.

DHFR, $DHFR_{4+}$ and $DHFR_{tag}$ constructs (Fig. 10) were built by deleting parts of the 10+ tag via whole plasmid PCR amplification followed by Xho I digestion and unimolecular ligation as follows: ~100 ng of the DHFR_10+ tag plasmid was amplified using 5 µM of dcr and delF (to produce DHFR), or 2dcF ($DHFR_{4+}$) or dcf ($DHFR_{tag}$) using Phire Hot Start II DNA polymerase (Finnzymes) in 100 µL final volume (pre-incubation at 98ºC for 30s, then cycling: denaturation at 98ºC for 5 s, extension at 72ºC for 1.5 min for 30 cycles, primer sequences see Table 5). PCR products were purified with QIAquick PCR Purification Kit (Qiagen), digested with Xho I (FastDigest, Fermentas) and ligated with T4 ligase (Fermentas). 0.6 µL of the ligation mixture was transformed into E. cloni® 10G cells (Lucigen) by electroporation. The transformed bacteria were selected overnight at 37ºC on ampicillin (100 µg/ml) LB agar plates. The identity of the clones was confirmed by sequencing.

Construction of N120D AlkB mutant

The AlkB gene was amplified using 120D (forward) and T7 terminator (reverse) primers (Table 5). The PCR conditions were: 0.3 mL final volume of PCR mix (150 µl of RED Taq ReadyMix, 6 µM of forward and reverse primers, ~400 ng of template plasmid), cycled for 27 times (after a pre-incubation step at 95ºC for 3 min, a cycling protocol was then applied: denaturation at 95ºC for 15 s, annealing at 55ºC for 15 s, extension at 72ºC for 3 min). The resulting PCR product was gel purified (QIAquick Gel Extraction Kit, Qiagen) and cloned into a pT7 expression plasmid (pT7-SC1) by MEGAWHOP procedure [Miyazaki, K. (2011) *Methods Enzymol* **498**, 399-406]: ~500 ng of the purified PCR product was mixed with ~300 ng of the WT AlkB circular DNA template and the amplification was carried out with Phire Hot Start II DNA polymerase (Finnzymes) in 50 µL final volume (pre-incubation at 98ºC for 30s, then cycling: denaturation at 98ºC for 5 s, extension at 72ºC for 1.5 min for 30 cycles). The circular template was eliminated by incubation with Dpn I (1 FDU) for 2 hr at

37ºC. 0.6 µL of the resulted mixture was transformed into 50 µL of E. cloni® 10G cells (Lucigen) by electroporation. The transformed bacteria were grown overnight at 37ºC on ampicillin (100 µg/ml) LB agar plates. The identity of the clones was confirmed by sequencing.

Purification of the strep-tagged AlkB-Fe^{++}

pT7-SC1 plasmids containing the strep-tagged AlkB gene were transformed into E. cloni® EXPRESS BL21(DE3) cells (Lucigen). Transformants were selected on LB agar plates supplemented with 100 µg/ml ampicillin grown overnight at 37°C. The resulting colonies were grown at 37°C (200 rpm shaking) in 2xYT medium supplemented with 100 µg/ml ampicillin until the O.D. at 600 nm was ~ 0.8. The cultures were then supplemented with 25 µM $FeSO_4$ and 100 µM L(+)-ascorbic acid (Merck) from fresh stock solutions (25 mM $FeSO_4$ and 100 mM L(+)-ascorbic acid in ddH_2O) and the protein expression was induced by supplementing with 0.5 mM IPTG. Bacteria were further grown overnight at 25°C, 200 rpm shaking. The next day the bacteria were harvested by centrifugation at 6000 x g at 4°C for 25 min. The resulting pellets were frozen at -80°C until further use.

AlkB-Fe^{++} was purified as following: bacterial pellets originating from 100 ml culture were resuspended in 30 ml lysis buffer (150 mM NaCl, 15 mM Tris.HCl pH 8.0, 1 mM $MgCl_2$, 0.2 units/ml DNase, 10 µg/ml lysozyme) supplemented with 5 µl β-mercaptoethanol (Merck) and 25 µM $FeSO_4$ and 100 µM L(+)-ascorbic acid, and incubated at RT for 20 min. Bacteria were further disrupted by probe sonication, and the crude lysate was clarified by centrifugation at 6000 x g at 4°C for 30 min. The supernatant was allowed to bind to ~150 µl (bead volume) of Strep-Tactin® Sepharose® (IBA) pre-equilibrated with the wash buffer (150 mM NaCl, 15 mM Tris.HCl pH 8.0) supplemented with 25 µM $FeSO_4$ and 100 µM L(+)-ascorbic acid, for 1 hr at 4°C ("end over end" mixing). Then the resin was loaded on a column (Micro Bio Spin, Bio-Rad) and washed with ~ 20 column volumes of the wash buffer supplemented with 25 µM $FeSO_4$ and 100 µM L(+)-ascorbic acid followed by ~ 3 column volumes of 150 mM NaCl, 15 mM Tris.HCl pH 8.0 (metal ions might interfere with the ClyA recordings, unpublished results, thus excess of iron was avoided). AlkB-Fe^{++} was subsequently eluted from the column in ~ 300 µl of elution buffer (150 mM NaCl, 15 mM Tris.HCl pH 8.0, 5 mM D-desthiobiotin (IBA)). Purified AlkB-Fe^{++} remained active for weeks, in agreement with the fact that self-inactivation of AlkB requires the presence of 2-OG.[32] The concentration of AlkB-Fe^{++} was measured using Bradford assay and the purity was checked using a 12% SDS-PAGE (Fig. 12).

Purification of the strep-tagged $DHFR_{n+}$

After transformation of pT7-SC1 plasmids containing the strep-tagged $DHFR_{n+}$ gene into E. cloni® EXPRESS BL21(DE3) cells (Lucigen), transformants were selected on LB agar plates supplemented with 100 µg/ml ampicillin after overnight growth at 37°C. The resulting colonies were grown at 37°C (200 rpm shaking) in 2xYT medium supplemented with 100 µg/ml ampicillin until the O.D. at 600 was ~ 0.8, after which $DHFR_{n+}$ expression was induced by addition of 0.5 mM IPTG, and subsequent switching to 25°C for overnight growth. The next day the bacteria were harvested by centrifugation at 6000 x g at 4°C for 25 min and the resulting pellets were frozen at -80°C until further use.

For purification, bacterial pellets originating from 100 ml culture were resuspended in 30 ml lysis buffer (150 mM NaCl, 15 mM Tris.HCl pH 7.5, 1 mM $MgCl_2$, 0.2 units/ml DNase, 10 µg/ml lysozyme) and incubated at RT for 20 min. Bacteria were further disrupted by probe sonication, and the crude lysate was clarified by centrifugation at 6000 x g at 4°C for 30 min. The supernatant was allowed to bind to ~150 µl (bead volume) of Strep-Tactin® Sepharose® (IBA) pre-equilibrated with the wash buffer (150 mM NaCl, 15 mM Tris.HCl pH 7.5) - "end over end" mixing. The resin was then loaded on a column (Micro Bio Spin, Bio-Rad) and washed with ~ 20 column volumes of the wash buffer. $DHFR_{n+}$ was subsequently eluted from the column in ~ 300 µl of elution buffer (150 mM NaCl, 15 mM Tris.HCl pH 7.5, 5 mM D-Desthiobiotin (IBA)). The concentration of $DHFR_{n+}$ was measured using Bradford assay and the purity was checked using a 12% SDS-PAGE (Fig. 13). Proteins were stored at 4°C (up to 3 weeks) until use.

ClyA-AS protein overexpression and purification

E. cloni® EXPRESS BL21 (DE3) cells were transformed with the pT7-SC1 plasmid containing the ClyA-AS gene. ClyA-AS contains eight mutations relative to the *S. Typhi* ClyA-WT: C87A, L99Q, E103G, F166Y, I203V, C285S, K294R and H307Y (the H307Y mutation is in the C-terminal hexahistidine-tag added for purification).[18] Transformants were selected after overnight growth at 37ºC on LB agar plates supplemented with 100 mg/L ampicillin. The resulting colonies were inoculated into 2xYT medium containing 100 mg/L of ampicillin. The culture was grown at 37ºC, with shaking at 200 rpm, until it reached an OD_{600} of ~ 0.8. The expression of ClyA-AS was then induced by the addition of 0.5 mM IPTG and the growth was continued at 25ºC. The next day the bacteria were harvested by centrifugation at 6000 x g for 25 min at 4°C and the pellets were stored at -80ºC.

The pellets containing monomeric ClyA-AS were thawed and resuspended in 20 mL of wash buffer (10 mM imidazole, 150 mM NaCl, 15 mM Tris.HCl, pH 8.0), supplemented with 1 mM $MgCl_2$ and 0.05 units/mL of DNase I and the bacteria were

lysed by sonication. The crude lysates were clarified by centrifugation at 6000 x g for 20 min at 4°C and the supernatant was mixed with 200 μL of Ni-NTA resin (Qiagen) in wash buffer. After 1 hr, the resin was loaded into a column (Micro Bio Spin, Bio-Rad) and washed with ~5 ml of the wash buffer. ClyA-AS was eluted with approximately ~0.5 mL of wash buffer containing 300 mM imidazole. Protein concentration was determined by the Bradford assay. Because ClyA-AS monomers were not active upon freezing, they were stored at 4°C until further use.

Type I ClyA-AS oligomers were obtained by incubation of ClyA-AS monomers with 0.5% β-dodecylmaltoside (DDM, GLYCON Biochemicals, GmbH) at 25ºC for 15 min. ClyA-AS oligomers were separated from monomers by blue native polyacrylamide gel electrophoresis (BN-PAGE, Bio-rad) using 4-20% polyacrylamide gels. The bands corresponding to Type I ClyA-AS were excised from the gel and were placed in 150 mM NaCl, 15 mM Tris.HCl pH 8.0 supplemented with 0.2% DDM and 10 mM EDTA to allow diffusion of the proteins out of the gel.

Electrical recordings in planar lipid bilayers

The applied potential refers to the potential of the *trans* electrode. ClyA-AS nanopores were inserted into lipid bilayers from the *cis* compartment, which was connected to the ground electrode. The two compartments were separated by a 25 μm thick polytetrafluoroethylene film (Goodfellow Cambridge Limited) containing an orifice of ~100 μm in diameter. The aperture was pretreated with ~5 μl of 10% hexadecane in pentane and a bilayer was formed by the addition of ~10 μL of 1,2-diphytanoyl-sn-glycero-3-phosphocholine (DPhPC) in pentane (10 mg/mL) to both electrophysiology chambers. Typically, the addition of 0.01-0.1 ng of oligomeric ClyA-AS to the *cis* compartment (0.5 mL) was sufficient to obtain a single channel. ClyA-AS nanopores displayed a higher open pore current at positive than at negative applied potentials, which provided a useful tool to determine the orientation of the pore. Electrical recordings were carried out in 150 mM NaCl, 15 mM Tris.HCl pH 8.0 (AlkB experiments) or 150 mM NaCl, 15 mM Tris.HCl pH 7.5 (DHFR experiments). The temperature of the recording chamber was maintained at 28°C by water circulating through a metal case in direct contact with the bottom and sides of the chamber.

Data recording and analysis

Electrical signals from planar bilayer recordings were amplified using an Axopatch 200B patch clamp amplifier (Axon Instruments) and digitized with a Digidata 1440 A/D converter (Axon Instruments). Data were recorded by using the Clampex 10.4 software (Molecular Devices) and the subsequent analysis was carried out with the Clampfit software (Molecular Devices). Electrical recordings were performed in 150 mM NaCl, 15 mM Tris.HCl pH 8.0 (AlkB) or pH 7.5 (DHFR) by applying a 2 kHz low-

pass Bessel filter and a 10 kHz sampling rate. For further analysis traces were filtered digitally with a Bessel (8-pole) low-pass filter with a 50 Hz cut-off. Residual current values ($I_{RES\%}$) were calculated from blocked pore current values (I_B) and open pore current values (I_O) as $I_{RES\%} = 100 * I_B / I_O$. I_B and I_O were determined from Gaussian fits to all point current histograms (0.05 pA bin size) for at least 15 individual protein blockades. $\Delta I_{RES\%}$ values were calculated from $I_{RES\%}$ using propagation of errors.

Current transitions from level 1 were analyzed with the "single-channel search" function in Clampfit. The detection threshold to collect the ligand-induced events for AlkB was set to 4 pA and events shorter than 10 ms were ignored. For NADP+ and "short" NADPH binding events to $DHFR_{tag}$:MTX, the detection threshold was also set to 4 pA and events shorter than 1 ms were neglected. The resulting event dwell times (t_{off}) and the time between events (t_{on}) were binned together as cumulative distributions and fitted to a single exponential to retrieve the ligand-induced lifetimes (τ_{off}) and the ligand-induced event frequencies ($f = 1/\tau_{on}$). The process of event collection was monitored manually. For AlkB, final values of τ_{on} and τ_{off} were based on average values derived from at least 3 single channel experiments at each concentration. Each experiment analysed more than 8 AlkB blockades. At the low ligand concentrations (0.2 mM) about 100 ligand-binding events were measured. Otherwise more than 150 events were collected. In total, 500 – 1200 events were considered for 2-OG, 350 – 2100 events for SUC (350 events were collected at the lowest concentration, all other concentrations more than 800 events) and 500 – 1300 events for N-OG. For $DHFR_{tag}$:MTX, > 500 NADPH and > 2000 NADP+ binding events were used in total to determine the values of τ_{on} and τ_{off}, where individual values for t_{on} and t_{off} were derived for at least five single channel experiments, each analysing more than 40 $DHFR_{tag}$:MTX blockades and more than 2000 ligand-binding events. Since the life time of the "long" NADPH binding events to $DHFR_{tag}$:MTX binary complex exceeded the residence time of the binary complex in the ClyA-AS nanopore (the dissociation of "long" NADPH was only occasionally observed), t_{off} values could not be determined. t_{on} values for NADPH were determined by collecting the times between the capture of the $DHFR_{tag}$:MTX binary complex in the nanopore and the transition to the ~4 pA higher current level within the same blockade lasting longer than 0.2 s. Subsequently, the t_{on} values were binned together as cumulative distributions and fitted to a single exponential fit to retrieve characteristic τ_{on} values. The values for k_{off} represented in Figure 2b and Figure 4b were determined by taking the average ± standard deviations of $1/t_{off}$ of at least 3 single channel experiments. The values of the association rate constants (k_{on}) were determined from the slope of the linear regression curves calculated from the dependency of the event frequencies ($f = 1/\tau_{on}$)

on the ligand concentration (OriginLab, Figs. 2b and 4b). Graphs were made with Origin (OriginLab Corporation) or Clampfit software (Molecular Devices).

Example 2: A demethylase as a protein adaptor

As a first model protein we selected *E. coli* AlkB demethylase (Mw=25 kDa), a globular protein that is expected to pass the *cis* entry of ClyA, but is too large to traverse the *trans* exit of the nanopore (Fig. 1a,b). In complex with iron ions (AlkB-Fe^{++}) AlkB co-oxidises methylated DNA and its cofactor 2-oxoglutarate (2-OG), producing succinate (SUC), carbon dioxide and formaldehyde (Aravind, L. & Koonin, E. V. (2001) *Genome biol.* **2**, RESEARCH0007; Trewick, S. C. (2002) *Nature* **419**, 174-178), 2-oxoglutarate is an important metabolite that influences aging and age-related diseases (Chin, R. M. et al. (2014) *Nature*, **510**, 397-401), and is a biomarker for non-alcoholic fatty liver disease (Rodriguez-Gallego, E. (2015) *Int. j. obesity* **39**, 279-287), heart failure and cardiorenal syndrome (Nikolaidou, T. et al. (2010) *Heart*, **96**, e14). The level of succinate in urine is a biomarker for kidney damage (Peti-Peterdi, J. (2014) US8652771).

Individual AlkB-Fe^{++} molecules were studied using Type I ClyA-AS (ClyA-AS hereafter). In 150 mM NaCl, 15 mM Tris HCl and pH 8.0 ClyA-AS formed nanopores with a steady open pore conductance (I_O = -1.7±0.1 nSi, average± SD, N=38, -60 mV, 28°C) under a wide range of applied potentials. Here and hereafter N indicates the number of independent single nanopore experiments, np the number of individual protein block-ades and nl the total number of ligand binding events analysed. The addition of AlkB-Fe^{++} (~4 nM) to the *cis* side of ClyA-AS provoked current blockades (I_B), quoted here as residual currents calculated as a percentage of the open pore current ($I_{RES\%}$), due to the electroosmotic confinement of AlkB-Fe^{++} between the wider *cis* entrance and the narrower *trans* exit of the protein nanopore (Fig. 1b)[18,20]. Conveniently, AlkB-Fe^{++} remained trapped inside the nanopore for several minutes (Fig. 1c). The signal induced by AlkB-Fe^{++} fluctuated between two distinctive current levels, L1 ($I_{RES\%}$ = 52.6±2.0%, n=15, N=7) and L2 ($I_{RES\%}$ = 39.0±1.0%, n_p =15, N=7, Fig. 1c), possibly due to two residence sites for the protein within the lumen of the ClyA-AS nanopores (Soskine, M. (2012) *Nano Lett.* **12**, 4895-4900).

At -60 mV the addition to the *cis* reservoir of the cofactor (2-OG), an isosteric inhibitor (N-oxalylglycine, N-OG) or the processed cofactor (SUC) induced reversible current enhancements within the AlkB-Fe^{++} blockades ($\Delta I_{RES\%}$= +4.7±1.3%, +4.9±1.0 and +4.6±1.3, respectively, n=15 AlkB blockades with each AlkB blockade typically n_p>15, n_l > 75 ligand binding events, N>4,N>4 single channel experiments, Fig. 2a, Figs. 5 and 6, and Table 1) that showed a mean duration (τ_{off}) of 1.7±0.5 s, 1.8±0.4

s and 61±11 ms, respectively (>4500 ligand binding events, N>8 single channel experiments, with each experiment typically analysing n>10 AlkB blockades).

Table 1. $I_{RES\%}$ values of AlkB-Fe^{++}-induced current blockades. All data were collected at -60 mV applied potential in 150 mM NaCl, 15 mM Tris.HCl pH 8.0 at 28°C. Values were calculated from 15 individual AlkB blockades. Errors are given as standard deviations. The ClyA-AS open-pore conductance (I_o) was 1.7±0.1 nSi (N=38 single channels). $\Delta I_{RES\%}$ is the difference between the $I_{RES\%}$ of the AlkB-Fe^{++} protein blockades and the $I_{RES\%}$ induced by the ligand (L1B or L2B). Proteins and ligands were added to the *cis* chamber.

	No ligand		2-OG		SUC		N-OG	
	L1 $I_{RES\%}$	L2 $I_{RES\%}$	L1B $\Delta I_{RES\%}$	L2B $\Delta I_{RES\%}$	L1B $\Delta I_{RES\%}$	L2B $\Delta I_{RES\%}$	L1B $\Delta I_{RES\%}$	L2B $\Delta I_{RES\%}$
AlkB-Fe^{++} WT	52.6 ±2.0%	39.0 ±1.02%	+4.7 ±1.3%	+1.7 ±1.2%	+4.6 ±1.3%	+2.1 ±1.0%	+4.9 ±1.0%	+1.7 ±1.0%
AlkB-Fe^{++} N120D	55.0 ±1.1%	39.3 ±1.24%	/	/	/	/	/	/

The current enhancements were also observed from the current level L2 (Fig. 6). We hypothesised that such current events reflected the conformational changes occurring during the transition from the open conformation of the apo-enzyme to the closed state of the ligand-bound form of AlkB-Fe^{++} (Fig. 2a) [Bleijlevens, B. et al. (2008) *EMBO rep.* **9**, 872-877; Bleijlevens, B. et al. (2012) *Biochem*. 2012, 51, 3334-3341]. To confirm this hypothesis we tested an AlkB mutant where the asparagine at position 120, which has been reported to be involved in the binding of 2-OG to AlkB, was substituted by aspartate (N120D). The addition of 7.2 mM of 2-OG did not induce current transitions to the N120D-AlkB-Fe^{++} blockades (N=4), suggesting that the affinity of this AlkB mutant for 2-OG is strongly reduced. As expected for a protein-ligand association process the dissociation rate constants (k_{off}, Table 2), measured from the inverse of the dwell times of the ligand-binding events ($1/\tau_{off}$), did not depend on the concentration of the ligand, while the frequencies of the ligand-induced events ($f = 1/\tau_{on}$) increased linearly with the concentration of the three ligands, from which slopes the association rate constants (k_{on}) could be calculated (Fig. 2b, Table 2).

Table 2. Kinetic parameters for ligand binding to AlkB-Fe^{++}. All data were collected in 150 mM NaCl, 15 mM Tris.HCl pH 8.0 at 28°C. Errors are given as standard deviations. Proteins and ligands were added to the *cis* chamber.

	2-OG	SUC	N-OG
k_{off}^{-60mV} (s^{-1})	0.66± 0.33	16.6± 2.6	0.57± 0.10
k_{on}^{-60mV} ($s^{-1}M^{-1}$)	1.8± 0.3 x 10^3	9.2± 1.3 x 10^2	1.2± 0.3 x 10^3

AlkB blockades

About 30% of the AlkB-Fe^{++}-induced current blockades did not show ligand-induced transitions, suggesting that the trapped enzymes might have a preferred orientation inside the ClyA-AS lumen. An alternative explanation is that sub-populations of AlkB-Fe^{++} might be inactive as a consequence of self-inactivation (Welford, R. W. et al. (2003) *J Biol Chem* **278**, 10157-10161), proteolysis, loss of iron, misfolding, etc. AlkB blockades not showing ligand-induced current transitions were ignored and the enzyme was ejected from the pore by reversing the potential to +60 mV. The AlkB-Fe^{++} blockades were nearly eliminated upon addition of 40 µM of cognate aptamer (Fig. 8, Table 5), indicating that, as previously reported for other proteins [Soskine (2012) cited above], AlkB-Fe^{++} formed complexes with the aptamer, which cannot be captured by ClyA nanopores as a result of electrostatic repulsion and/or steric hindrance (Franceschini, L. et al. (2013) *Nat. Comm.* **4**, 2415). This suggests that the majority of captured AlkB proteins are natively folded, as such aptamer was evolved to bind to folded AlkB (Krylova, S. M. et al. (2011) *Anal Biochem* **414**, 261-265).

Example 3: A reductase as a protein adaptor

E. coli dihydrofolate reductase (DHFR, Mw= 19 kDa) was selected as a second model protein adaptor (Fig. 3a,b). During the DHFR catalytic cycle dihydrofolate is reduced to tetrahydrofolate and the cofactor NADPH is oxidised to NADP+. Tetrahydrofolate is a cofactor in many metabolic reactions, thus inhibitors of DHFR such as methotrexate (MTX) are antibiotic and anticancer agents. The ratio of the NADP+ and NADPH intracellular concentrations is used to monitor the oxidative stress in cells (Ogasawara, Y. et al. (2009) *Biol. & pharmaceut. bull.* **32**, 1819-1823). We found that apo-DHFR, which is smaller than AlkB, dwelled inde ClyA-AS only for a few milliseconds. Upon the addition of MTX to the *cis* solution the frequency and the dwell time of the protein blockades decreased, while the residual current increased. The blockades were then abolished by the subsequent addition of NADPH to the same

side (Fig. 11). Since both the inhibitor and the cofactor are negatively charged, these results suggested that the additional negative charges increased the electrophoretic/electrostatic drag force opposing DHFR entry and residence inside the nanopore. In order to increase the residence time of the protein, we engineered DHFR by introducing a polypeptide tag containing four additional positive charges at the C-terminus of the protein ($DHFR_{tag}$, Fig. 10). In complex with MTX, $DHFR_{tag}$, added to the *cis* compartment, induced current blockades with a mean dwell of 3.1±1.4 s (N=5, n_p=230,, Fig. 3c) that was three orders of magnitude longer than $DHFR_{tag}$ or DHFR:MTX blockades mean dwell times. A possible explanation to this result is that, tuned by the additional positive charges, the binary $DHFR_{tag}$:MTX complex is at a potential minimum inside the nanopore where the electroosmotic, electrophoretic and electrostatic forces are balanced. The dissociation of MTX from the binary complex was slower than the residence time of the complex inside the nanopore and could not be observed by ionic current recordings. As shown before with apo-AlkB-Fe^{++}, $DHFR_{tag}$:MTX blockades showed a main current level L1 ($L1_M$, $I_{RES\%}$ = 74.7±0.5%, n_p =25, N=5) that rarely visited a second current level L2 ($L2_M$, $I_{RES\%,}$ = 53.5±0.9%, n_p =25, N=5, Fig. 3c).

At −90 mV the addition of the oxidised cofactor NADP+ to the *trans* compartment of ClyA-AS produced reversible current enhancements to the $DHFR_{tag}$:MTX complex blockades formed in the *cis* solution ($L1_{M:N+}$, $\Delta I_{RES\%}$= +2.3±0.5%, n_p = 15 blockades, n_I > 225, N=3; and $\tau_{M:N+}$ = 102±11 ms, n_I = 19,000, N=9 n_p > 800, Fig. 4a, Table 3, Fig. 7). Association and dissociation rate constants could be measured from titration experiments (Fig. 4b, Table 4).

NADPH added to the *trans* compartment also induced additional current enhancements to the binary complex blockades (Fig. 4a). Remarkably, the current events induced by NADPH showed a slightly higher residual current ($L1_{M:NH}$, $\Delta I_{RES\%}$= +2.7±0.7%, n_p = 15 n_I=15, N=4, Table 3) than the NADP+ blockades ($\Delta I_{RES\%}$= +2.3±0.5%) and had a dwell time longer than the residence time of the ternary complex inside the nanopore (Fig. 4a). As a consequence, despite the minute difference between NADPH and NADP+ (a hydride ion), the binding of the two ligands to $DHFR_{tag}$:MTX could be clearly differentiated (Fig. 4a).

Table 3. $I_{RES\%}$ values of $DHFR_{tag}$:MTX ligand-induced current blockades. All data were collected at -90 mV applied potential in 150 mM NaCl, 15 mM Tris.HCl pH 7.5 at 28°C. Values were calculated from at least 15 individual $DHFR_{tag}$:MTX blockades. Errors are given as standard deviations. The ClyA-AS open-pore conductance (I_o) was 1.6±0.1 nSi (N=15 single channels). $\Delta I_{RES\%}$ is the difference between the $I_{RES\%}$ of the $DHFR_{tag}$:MTX blockades and the $I_{RES\%}$ induced by the ligand (L1B or L2B). 50 nM of $DHFR_{tag}$ and 400 nM MTX were added to the *cis* chamber, NADPH and NADP+ were added to the *trans* chamber.

	No ligand		NADP+		NADPH	
	L1 $I_{RES\%}$	L2 $I_{RES\%}$	L1B $\Delta I_{RES\%}$	L2B $\Delta I_{RES\%}$	L2B $\Delta I_{RES\%}$	L2B $\Delta I_{RES\%}$
$DHFR_{tag}$:MTX	74.7±0.5 %	53.5±0.9 %	+2.3±0 .5%	+4.7±0 .9%	+2.7±0 .7%	+5.4±1 .0%

Table 4. Kinetic parameters for ligand binding to $DHFR_{tag}$:MTX. All data were collected in 150 mM NaCl, 15 mM Tris.HCl pH 7.5 at 28°C. Errors are given as standard deviations. 50 nM of $DHFR_{tag}$ and 400 nM MTX were added to the *cis* chamber, NADPH and NADP+ were added to the *trans* chamber.

	NADP+	NADPH
k_{off},$^{-90mV}$ (s^{-1})	10±1	NA
k_{on},$^{-90mV}$ ($s^{-1}M^{-1}$)	2.1±0.3 x 10^6	4.8±1.2 x 10^6

Although the bulk kinetic constants for the binding of NADP+ and NADPH to MTX:DHFR could not be retrieved from the literature, the equilibrium dissociation constant for the binding of 2-OG to AlkB-Mn^{++} was recently measured by an intrinsic tryptophan fluorescence quenching assay (K_D^{bulk}= 4.1±0.6 10^{-6} M at 24 °C) (Ergel, B. et al. (2014) *J biol chem* ***289***, 29584-29601). By comparison, the equilibrium dissociation constant of 2-OG for AlkB-Fe^{++} inside the nanopore measured from the ratio of the association and dissociation constants ($K_D^{pore} = k_{off}/k_{on}$) was about two orders of magnitude higher than the bulk value (K_D^{pore}=3.7±1.9 10^{-4} M, -60 mV, 28°C). This effect is likely to be related to the confinement of AlkB-Fe^{++} inside the nanopore and to the effect of the applied potential. ClyA nanopores have a negatively charged interior and are, therefore, cation selective (Ludwig, A. et al. (1999) *Mol. Microbiol.* **31**, 557-567). Thus, under negative applied potentials (*trans*) the diffusion of the negatively charged ligands added to the *cis* solution through the nanopore is likely to be opposed. This is probably to be further accentuated by the unfavourable electrostatic interaction between the ligands and the wall of the nanopore lumen. This complication might be overcome by using nanopores with an internal charge with an opposite sign to

Heterogeneities in $DHFR_{tag}$:MTX blockades and NAPDH binding events

Approximately 45% of the $DHFR_{tag}$:MTX blockades did not respond to the addition of NADP+ (added in *trans*, Fig. 9c,d). Since all the observed $DHFR_{tag}$ molecules captured by ClyA-AS were bound to MTX, this effect is not likely due to misfolded DHFR molecules. Besides, when NADPH was added to the *trans* chamber, two distinct populations of $DHFR_{tag}$:MTX blockades were observed: the first (~55% of blockades) gave rise to NADPH binding events with a lifetime longer than the residence time of the complex within ClyA-AS (lifetime >3 seconds, "long" NADPH events), the second population (~45% of blockades) corresponded to $DHFR_{tag}$:MTX blockades that displayed NADPH binding events with a lifetime of 38.5±0.8 ms ("short" NADPH events). Most blockades showed either "long" or "short" NADPH events (Fig. 9a). Rarely, however, the same $DHFR_{tag}$:MTX blockade switched between the two NADPH binding behaviours (Fig. 9b). "Long" and "short" NADPH events showed similar association rate constants (k_{on} = 4.8 ±1.2 $s^{-1}\mu M^{-1}$ and k_{on} = 5.8±1.2 $s^{-1}\mu M^{-1}$, respectively) and similar $\Delta_{IRES\%}$ values (2.7±0.7% and 2.2±0.9%, respectively, Fig. 9a,b). Although "short" NADPH binding events could arise from NADP+ contaminations, this is unlikely since fresh NADPH aliquots (>95% purity) were used for every experiment. Furthermore, the lifetime of "short" NADPH events was significantly shorter than the lifetime of NADP+ events. In addition, the fact that most of the $DHFR_{tag}$:MTX blockades showed only one binding behaviour, suggests that the observed heterogeneity is not arising from impurities in the substrate samples but from heterogeneity in the protein adaptor (Fig. 9). This variability in binding behaviour could then arise from different configurations of $DHFR_{tag}$:MTX inside the ClyA-AS nanopore and/or from different conformations of the $DHFR_{tag}$:MTX complex. Although the first hypothesis cannot be easily tested, it is interesting to note that previous studies revealed that MTX can bind to two different DHFR conformations with different binding affinities towards NADP+ and NADPH (Rajagopalan, P. T. et al. (2002) *Proc Natl Acad Sci USA* **99**, 13481-13486).

Tailoring the DHFR nanopore adaptor for optimal nanopore residence

Our initial DHFR construct consisted of DHFR from *E. coli* with the cysteine residues at positions 85 and 152 substituted with alanine and serine, respectively, and with a C-terminal Strep-tag, inserted for purification purposes, spaced by a 9 amino acid long linker (see later). The fusion tag polypeptide chain contained one additional net positive charge with respect to the wild type sequence (originating from the introduction of a Xho I restriction site in the DNA sequence of the protein). The

addition of DHFR (50 nM, Fig. 10) to the *cis* compartment induced transient blockades to the ClyA-AS open pore current with $I_{RES\%}$ of 71.5±0.8 % and a lifetime of 21±2 ms (n=200 blockades, N=4 single channels) under –90 mV applied potential (Fig. 11a, left). Subsequent addition of 400 nM of MTX to the *cis* compartment resulted in blockades with increased $I_{RES\%}$ values ($I_{RES\%}$=78.4±0.6%) and decreased lifetime (3.3±0.7 ms, n=300 blockades, N=3 single channels, Fig. 11a, centre). Further addition of 20 μM NADPH to the same compartment resulted in the nearly total elimination of the DHFR blockades (Fig. 11a, right), suggesting that the DHFR:MTX:NADPH complex was mostly excluded from the ClyA-AS nanopore. Thus, although we could observe the interaction between the ligands and DHFR, the protein did not remain inside the ClyA-AS nanopore for a time long enough to determine the binding kinetics, prompting us to design DHFR constructs that would have a longer residence time within the ClyA-AS nanopore.

In order to increase the residence time of DHFR into ClyA, we have designed and tested three DHFR constructs that were decorated with a different number of positive charges incorporated into flexible C-terminal fusion tags. We expected the additional charges would prolong the dwell times of the ternary complex within the ClyA-AS nanopore because of the decreased electrostatic repulsion between the negatively charged protein (the pI of DHFR is 4.8) and the negatively charged nanopore lumen (Soskine (2013), cited above), and the reduced electrophoretic drag on DHFR under negative applied potentials. Initially we tested $DHFR_{10+}$, which consisted of the DHFR gene with a C-terminal recombinant tag baring 10 net positive charges with respect to wild type DHFR. The sequence of the 10+ tag comprised of a S-tag (KETAAAKFERQHMDS) (SEQ ID NO:16) derived from pancreatic RNase A, followed by a positively charged coil (KIAALKQKIAALKYKNAALKKKIAALKQ, adapted from Ref. 40) (SEQ ID NO: 17) (Table 6) and, a Strep-tag for easy purification. DHFR and the three tags were spaced by flexible linkers (Fig. 10). Since we could not predict what would be the effect of the positively charged tag and linker length on the DHFR blockades, we have also designed two constructs with shorter tags and smaller number of additional positive charges: $DHFR_{4+}$ and $DHFR_{tag}$ baring 4 and 5 net positive charges, respectively (Fig 10).

$DHFR_{10+}$, $DHFR_{4+}$ and $DHFR_{tag}$ induced fast current blockades to ClyA-AS nanopores that converted into second-long blockades upon binding to MTX (Fig. 11). $DHFR_{10+/4+/tag}$:MTX blockades were remarkably longer than DHFR:MTX blockades (e.g. the lifetime of $DHFR_{tag}$:MTX blockades was ~1000 fold that of DHFR:MTX blockades), indicating that the positively charged tags efficiently counterbalanced the electrostatic and electrophoretic effects induced by MTX binding (Fig. 11). Although

the blockades induced by the $DHFR_{10+/4+/tag}$:MTX complexes reported the binding of NADPH through ~4 pA enhancements of the residual ionic current (Fig. 11b,c,d, right), $DHFR_{10+}$ and $DHFR_{4+}$ blockades produced non-ideal output signals. The residual current of $DHFR_{10+}$ blockades often switched to a level of lower conductance (Fig. 11b, centre and right), while the binding of NADPH to $DHFR_{4+}$:MTX prompted the quick release of the complex from the pore, indicating that 4 additional positive charges are not enough to keep ternary complex within the pore (Fig. 11c, right). On the other hand, $DHFR_{tag}$:MTX:NADPH was internalised for sufficient time for accurate kinetic analysis and therefore it was chosen for thorough characterization as our nanopore-adaptor.

Example 5 Detection of analytes with Venus flytrap domains

Venus flytrap domain family of periplasmic binding proteins (PBP) might provide ideal protein adaptors because: 1) they have a domain that has an elongated shape that appears to fit well inside the nanopore and provides a quiet blocked pore signal (Fig. 14). 2) the domain comprises two lobes that upon binding close on the substrate through a large conformational change. 3) Periplasmic binding proteins (PBPs) scavenge or sense diverse nutrients in the environment by coupling to transporters in the inner cell membrane, thus they bind physiologically or technologically relevant substrates with high affinity and selectivity. 4) They bind hundreds of substrates and metabolites (B12 vitamin, many sugars, amino acids, neurotransmitters, etc).
5) Substrate binding appears to be modulated by an 8 residue motif, thus targeted mutations might allow tuning the selectivity for target analytes to the experimental needs.

Results

sensor for asparagine

The interaction of SBD1 with asparagine was sampled using type I ClyA-AS nanopores. ClyA-AS (C87A/ L99Q/ E103G/ F166Y/ I203V/ C285S/ K294R/H307Y). In 150 mM NaCl and 15 mM Tris-HCl (pH 7.5), the addition of 74 nM of SBD1 to the *cis* compartment of Type I ClyA-AS induced transient current blockades at negative applied potentials (*trans*). At -60 mV the blockades showed one main level (Level I, Figure 15A,B) with a residual current ($I_{res\%}=I_B/I_0$ x 100) of $I_{res\%}$ = 67.6 ± 0.1 % (N=5). Every 3.5 ± 0.1 s^{-1} (mean± S.E., n= 212) the current switched to Level II ($I_{res\%}$= 66.8 ± 0.4 %, N=5) with a lifetime of 109 ± 1 ms (mean ± S.E., n=340). The protein blockades released spontaneously after 4.2 ± 1.8 s (mean± S.E., n=291). Upon addition of asparagine (concentrations ranging from 200 nM to 4 µM, Figure

15B), the frequency of the level II increased (Fig. 15B), suggesting that the current blockades are due to the binding of arginine to the SBD1 adaptor inside the nanopore. An inactive SBD1 variant, containing the mutation E184W showed similar blockades to Type I ClyA-AS pores at -60 mV ($I_{res\%}$ = 66.7). However, addition of up to 1 mM asparagine did not show any Level II blockades, indicating that Level II blockades confirming to the asparagine-bound or closed conformation of SBD1.

The dissociation constant was determined by titrating the substrate and plotting the relative closed population (CL/(O+ CL)), determined from the area of the all point current histogram, versus the concentration. Fitting this curve to a one-site binding isotherm gave a K_d value of 0.47 ± 0.03 μM (Figure 15C), which is in agreement with previously described values obtained by smFRET and isothermal titration calorimetry (ITC) (Gouridis, G. et al. (2015) *Nature struct. & mol. biol.* **22**, 57-64) . The closing and opening rate constants were determined from the inverse of the open and closed state lifetimes respectively and were plotted versus the asparagine concentration. The closing rate was linearly dependent on the substrate concentration and the slope of the linear fit gave the $k_{closing}$ = 1.2 x 10^7 s^{-1} M^{-1}. The opening rate constant did not show concentration dependency and the value of $k_{opening}$ was determined by the intercept at zero 9.4 s^{-1} (Figure 15D).

sensor for glutamine

The interaction of SBD2 with glutamine was sampled using type I ClyA-AS nanopores at -100 mV. The addition of 72 nM of SBD2 induced a current blockade that fluctuated between two levels I ($I_{res\%}$ = 63.6 ± 0.3 %, τ = 256 ± 5 ms, N=3) and level III ($I_{res\%}$ = 61.0 ± 0.2 %, τ = 145 ± 13 ms, N=3). Protein blockades remained inside the nanopore for 3.9 ± 0.7 s (mean±S.E., n=225). Rarely the current visited an additional ionic current level, Level II ($I_{res\%}$ = 62.5 ± 0.3 %, τ = 18 ± 1 ms, n=856, N=3).

We studied ligand binding by stepwise addition of glutamine at concentrations ranging from 200 nM to 3 μM. After addition of glutamine, the frequency of level II increased linearly with the concentration of glutamine, suggesting this level is the glutamine-bound state. Addition of up to 200 μM glutamine to the SBD2(D417F), a variant that cannot close, did not show any Level II blockades; although conversion between Level I and Level II were still observed (Figure 17A). These results further suggests that Level II corresponds to the glutamine-bound (Figure 16A), while the levels I and III might represent different configurations of the protein inside the nanopore. Binding rates were determined from the lifetimes as described above. Upon linear fitting of the binding rate curve the glutamine binding rates from Level I

and III were determined. Glutamine binding from Level I showed a nearly identical on rate (k_{on} = 3.7 x 10^7 s^{-1} M^{-1}) as binding from Level II (k_{on} = 3.8 x 10^7 s^{-1} M^{-1}, Figure 3C). The opening rate constant was determined by the intercept at zero k_{off} = 39.7 s^1. The obtained K_d value of glutamine binding to SBD2 (1.27 ± 0.14 µM, Figure 16B) is in agreement with previously described values obtained by smFRET and ITC (Gouridis, G. et al. (2015) *Nature struct. & mol. biol.* **22**, 57-64).

Glucose sensor

Preliminary results showed that the venus flytrap domain of a glucose binding protein (GBP) from *E. coli* might be a good protein adaptor for a glucose sensor. GBP showed a low background signal (Fig. 18) and an average residence time of ~2 s. Interestingly, in the absence of ligand we observed two current levels, which probably reflected the open and closed conformation of the protein (Fig. 18b-c). The addition of glucose to the *cis* solution increased the dwell time of one level (presumably the closed state, Fig. 18), suggesting that the conformational changes associated with the binding of ligands to the nanopore can be observed. According to the U.S.FDA recommendations, glucose sensors should detect glucose concentrations between 1.65 and 22 mM (Yoo, E.-H. & Lee, S.-Y. (2010) *Sensors* **10**, 4558-4576). The sensitivity of GBP for glucose is ~1000 fold higher, suggesting that in a few seconds a GBP-based sensor could measure the concentration of glucose in blood. Further, glucose could be also measured in other body fluids such as saliva or sweat, where glucose concentration is much lower (8-210 µM[4] and 0.277–1.11 mM, respectively (Makaram, P. et al. (2014) *Diagnostics* **4,** 27-46; Moyer, J. et al. (2012) *Diabetes Technology & Therapeutics* **14**, 398-402). A device based on GBP would not require 'finger pricking'.

Example 6. Effect of ClyA mutants on protein recognition

Several mutations inside the ClYA-AS nanopore (Fig. 19) were tested to find out which location within the nanopore allows better recognition. As a model system we used human thrombin (HT). When added on the cis side of the nanopore, HT enters the pore and switches between L1 and L2 binidng sites (Fig. 19B). At high applied potential L2 is populated more than L1 (Fig. 19c). To test the recognition point in ClyA-AS, we substituted a tryptophan residue (W) to several position inside the nanopore (Fig. 19A). The occupancy of L1 and L2 at different potentials depended on the mutant tested (Fig. 19C). Substitutions at position 49, 56 and 60 had the strongest effect, revealing the potential binding site for HT inside the nanopore.

In addition the binding of analytes to a protein lodged inside the nanopore was tested (Fig. 20A, SBD2).

We found that the recognition of the substrate is enhanced by placing a tryptophan residue at position 56. Lysine residues at position 56 or 60 reduced recognition.

Example 7 Primer and aptamer sequences disclosed in the invention

Primer name	Sequence	SEQ ID NO
fAlkB	AGATATAGCCATGGCGTTGGATCTGTTTGCCGATGCTGAAC	SEQ ID NO:22
AlkBr1	CGGATGGCTCCACGCGCTGCCTTCTTTTTTACCTGCCTGACGGAATG	SEQ ID NO:23
AlkBr2	TATATATAAGCTTATCATTTTTCAAACTGCGGATGGCTCCACGCGCTGCC	SEQ ID NO:24
120D	GCCAGATGCTTGTCTTATCAACCGCTACGCTCCTGGCGCGAAACTGTCGC	SEQ ID NO:25
T7-terminator	GCTAGTTATTGCTCAGCGG	SEQ ID NO:26
Anti-AlkB aptamer	TGCCTAGCGTTTCATTGTCCCTTCTTATTAGGTGATAATA	SEQ ID NO:27
DHf	atatatatatCCATGGCTTCGGCTATGATTTCTCTGATTGCG	SEQ ID NO:28
DHr	CGCGGTTTCTTTCGCTCGAGTACTGCTGCCacggcgttccaggatttcgaatgag	SEQ ID NO:29
Cof	ctcattcgaaatcctggaacgccgtGGCAGCAGTACTCGAGCGAAAGAAACCGCG	SEQ ID NO:30
Cor	atatatatatAAGCTTATCATTTTTCAAACTGCGGATGGC	SEQ ID NO:31
dcr	atatatatatCTCGAGTACTGCTGCCACGGCGTTCCAGGATTTCG	SEQ ID NO:32
delF	atatatatatCTCGAgcgggcAGCGCGTGGAGCCATCCGCAGTTTG	SEQ ID NO:33
2dcF	atatatatatCTCGAGCGaagaagattgcggccctaaaacaggg	SEQ ID NO:34
dcf	atatatatatCTCGAGCGaaaaagaagattgcggccctaaaacaggg	SEQ ID NO:35

Description	Sequence
Protein sequence for *S. typhi* ClyA (ClyA-WT) SEQ ID NO:1	MIMTGIFAEQTVEVVKSAIETADGALDLYNKYLDQVIPWKTFDETIKELSRFKQEYSQEASVLVGDIKVLLMDSQDKYFEATQTVYEWCGVVTQLLSAYILLFDEYNEKKASAQKDILIRILDDGVKKLNEAQKSLLTSSQSFNNASGKLLALDSQLTNDFSEKSSYFQSQVDRIRKEAYAGAAAGIVAGPFGLIISYSIAAGVIEGKLIPELNNRLKTVQNFFTSLSATVKQANKDIDAAKLKLATEIAAIGEIKTETETTRFYVDYDDLMLSLLKGAAKKMINTCNEYQQRHGKKTLFEVPDV
Protein sequence for ClyA with	MTGIFAEQTVEVVKSAIETADGALDLYNKYLDQVIPWKTFDETIKELSRFKQEYSQEASVLVGDIKVLLMDSQDKYFEATQTVYEWCGVVTQLLSAYIQLFDGYNEKKASAQKDILIRILDDGVKKLNEAQKSLLTSSQSFNNA

C285S substitution (ClyA-CS) SEQ ID NO:2	SGKLLALDSQLTNDFSEKSSYYQSQVDRIRKEAYAGAAAGIVAGPFGL IISYSIAAGVIEGKLIPELNNRLKTVQNFFTSLSATVKQANKDIDAAKLK LATEIAAIGEIKTETETTRFYVDYDDLMLSLLKGAAKKMINTSNEYQQR HGRKTLFEVPDVGSSHHHHHH*
Protein sequence for ClyA-AS SEQ ID NO:3	MTGIFAEQTVEVVKSAIETADGALDLYNKYLDQVIPWKTFDETIKELSR FKQEYSQEASVLVGDIKVLLMDSQDKYFEATQTVYEWAGVVTQLLSA YIQLFDGYNEKKASAQKDILIRILDDGVKKLNEAQKSLLTSSQSFNNA SGKLLALDSQLTNDFSEKSSYYQSQVDRIRKEAYAGAAAGIVAGPFGL IISYSIAAGVVEGKLIPELNNRLKTVQNFFTSLSATVKQANKDIDAAKL KLATEIAAIGEIKTETETTRFYVDYDDLMLSLLKGAAKKMINTSNEYQQ RHGRKTLFEVPDVGSSYHHHHH*
Nucleotide sequence for *S. typhi* ClyA SEQ ID NO: 4	CCTGCGTAGATAAGCAGGAAGCAGGCAGTATTTCCAGCTTCTGGAA TGTTAAAGCTACAAAAGTTGTCTGGAGGTAATAGGTAAGAATACTTT ATAAAACAGGTACTTAATTGCAATTTATATATTTAAAGAGGCAAATG ATTATGACCGGAATATTTGCAGAACAAACTGTAGAGGTAGTTAAAA GCGCGATCGAAACCGCAGATGGGGCATTAGATCTTTATAACAAATA CCTCGACCAGGTCATCCCCTGGAAGACCTTTGATGAAACCATAAAA GAGTTAAGCCGTTTTAAACAGGAGTACTCGCAGGAAGCTTCTGTTT TAGTTGGTGATATTAAAGTTTTGCTTATGGACAGCCAGGACAAGTAT TTTGAAGCGACACAAACTGTTTATGAATGGTGTGGTGTCGTGACGC AATTACTCTCAGCGTATATTTTACTATTTGATGAATATAATGAGAAAA AAGCATCAGCCCAGAAAGACATTCTCATTAGGATATTAGATGATGG TGTCAAGAAACTGAATGAAGCGCAAAAATCTCTCCTGACAAGTTCA CAAAGTTTCAACAACGCTTCCGGAAAACTGCTGGCATTAGATAGCC AGTTAACTAATGATTTTTCGGAAAAAAGTAGTTATTTCCAGTCACAG GTGGATAGAATTCGTAAGGAAGCTTATGCCGGTGCTGCAGCCGGC ATAGTCGCCGGTCCGTTTGGATTAATTATTTCCTATTCTATTGCTGC GGGCGTGATTGAAGGGAAATTGATTCCAGAATTGAATAACAGGCTA AAAACAGTGCAAAATTTCTTTACTAGCTTATCAGCTACAGTGAAACA AGCGAATAAAGATATCGATGCGGCAAAATTGAAATTAGCCACTGAA ATAGCAGCAATTGGGGAGATAAAAACGGAAACCGAAACAACCAGA TTCTACGTTGATTATGATGATTTAATGCTTTCTTTATTAAAAGGAGCT GCAAAGAAAATGATTAACACCTGTAATGAATACCAACAAAGACACG GTAAGAAGACGCTTTTCGAGGTTCCTGACGTCTGATACATTTTCATT CGATCTGTGTACTTTTAACGCCCGATAGCGTAAAGAAAATGAGAGA CGGAGAAAAAGCGATATTCAACAGCCCGATAAACAAGAGTCGTTAC CGGGCTGACGAGGTTATCAGGCGTTAAGCTGGTAG
Nucleotide sequence for ClyA with C285S substitution (ClyA-CS) SEQ ID NO: 5	ATGACGGGTATCTTTGCGGAACAGACGGTGGAAGTTGTGAAAAGT GCGATTGAAACGGCTGACGGTGCGCTGGACCTGTATAATAAATATC TGGATCAGGTCATCCCGTGGAAAACCTTTGACGAAACGATTAAAGA ACTGAGCCGTTTCAAACAGGAATACAGTCAAGAAGCGTCCGTCCTG GTGGGCGATATCAAAGTGCTGCTGATGGATTCTCAGGACAAATATT TTGAAGCTACCCAAACGGTTTACGAATGGTGTGGTGTGGTTACCCA GCTGCTGTCCGCATATATTCAGCTGTTCGATGGATACAACGAGAAA AAAGCGAGCGCGCAGAAAGACATTCTGATCCGCATTCTGGATGAC GGCGTGAAAAAACTGAATGAAGCCCAGAAATCGCTGCTGACCAGC TCTCAATCATTTAACAATGCCTCGGGTAAACTGCTGGCACTGGATA GCCAGCTGACGAACGACTTTTCTGAAAAAAGTTCCTATTACCAGAG CCAAGTCGATCGTATTCGTAAAGAAGCCTACGCAGGTGCCGCAGCA GGTATTGTGGCCGGTCCGTTCGGTCTGATTATCTCATATTCGATTG CTGCGGGCGTTATCGAAGGTAAACTGATTCCGGAACTGAACAATCG TCTGAAAACCGTTCAGAACTTTTTCACCAGTCTGTCTGCTACGGTCA

	AACAAGCGAATAAAGATATCGACGCCGCAAAACTGAAACTGGCCAC GGAAATCGCTGCGATTGGCGAAATCAAAACCGAAACGGAAACCAC GCGCTTTTATGTTGATTACGATGACCTGATGCTGAGCCTGCTGAAA GGTGCCGCGAAGAAAATGATTAATACCTCTAATGAATATCAGCAGC GTCACGGTAGAAAAACCCTGTTTGAAGTCCCGGATGTGGGCAGCA GCCACCACCATCATCACCACTAAAAGCTTGGATCCGGCTGCTAACA AAGCCCGAA
Nucleotide sequence for ClyA-AS SEQ ID NO:6	ATGACGGGTATCTTTGCGGAACAGACGGTGGAAGTTGTGAAAAGT GCGATTGAAACGGCTGACGGTGCGCTGGACCTGTATAATAAATATC TGGATCAGGTCATCCCGTGGAAAACCTTTGACGAAACGATTAAAGA ACTGAGCCGTTTCAAACAGGAATACAGTCAAGAAGCGTCCGTCCTA GTGGGCGATATCAAAGTGCTGCTGATGGATTCTCAGGACAAATATT TTGAAGCTACCCAAACGGTTTACGAATGGGCGGGTGTGGTTACCCA GCTGCTGTCCGCATATATTCAGCTGTTCGATGGATACAATGAGAAA AAAGCGAGCGCGCAGAAAGACATTCTGATCCGCATTCTGGATGAC GGCGTGAAAAAACTGAATGAAGCCCAGAAATCGCTGCTGACCAGC TCTCAATCATTTAACAATGCCTCGGGTAAACTGCTGGCACTGGATA GCCAGCTGACGAACGACTTTTCTGAAAAAAGTTCCTATTACCAGAG CCAAGTCGATCGTATTCGTAAAGAAGCCTACGCAGGTGCCGCAGCA GGTATTGTGGCCGGTCCGTTCGGTCTGATTATCTCATATTCAATTGC TGCGGGCGTTGTCGAAGGTAAACTGATTCCGGAACTGAACAATCGT CTGAAAACCGTTCAGAACTTTTTCACCAGTCTGTCTGCTACGGTCAA ACAAGCGAATAAAGATATCGACGCCGCAAAACTGAAACTGGCCACG GAAATCGCTGCGATTGGCGAAATCAAAACCGAAACGGAAACCACG CGCTTTTATGTTGATTACGATGACCTGATGCTGAGCCTGCTGAAAG GTGCCGCGAAGAAAATGATTAATACCTCTAATGAATATCAGCAGCG TCACGGTAGAAAAACCCTGTTTGAAGTCCCGGATGTGGGCAGCAG CTACCACCATCATCACCACTAAAAGCTT
AlkB-streptag (protein sequence, additional amino acid residues are underlined) SEQ ID NO:7	MALDLFADAEPWQEPLAAGAVILRRFAFNAAEQLIRDINDVASQSPFR QMVTPGGYTMSVAMTNCGHLGWTTHRQGYLYSPIDPQTNKPWPAM PQSFHNLCQRAATAAGYPDFQPDACLINRYAPGAKLSLHQDKDEPDL RAPIVSVSLGLPAIFQFGGLKRNDPLKRLLLEHGDVVVWGGESRLFYH GIQPLKAGFHPLTIDCRYNLTFRQAGKKEGSAWSHPQFEK**
> AlkB-streptag (DNA sequence) SEQ ID NO:8	Atggcgttggatctgtttgccgatgctgaaccgtggcaagagccactggcggctggtgc ggtaattttacggcgttttgcttttaacgctgcggagcaactgatccgcgatattaatgac gttgccagccagtcgccgtttcgccagatggtcacccccgggggatataccatgtcggt ggcgatgaccaactgtgggcatctgggctggacgacccatcggcaaggttatctctatt cgcccattgatccgcaaacaaataaaccgtggcccgccatgccacagagttttcataatt tatgtcaacgtgcggctacggcggcgggctatccagatttccagccagatgcttgtctta tcaaccgctacgctcctggcgcgaaactgtcgctgcatcaggataaagacgaaccgga tctgcgcgcgccaattgtttctgtttctctgggcttacccgcgatttttcaatttggcggcct gaaacgaaatgatccgctcaaacgtttgttgttggaacatggcgatgtggtggtatggg gcggtgaatcgcggctgttttatcacggtattcaaccgttgaaagcggggtttcatccact caccatcgactgccgctacaacctgacattccgtcaggcaggtaaaaaagaaggcagc gcgtggagccatccgcagtttgaaaaatgatAAGCTT
> $DHFR_{10+}$ (DNA sequence)	Atggcttcggctatgatttctctgattgcggcactggctgtcgatcgtgttattggtatgga aaacgctatgccgtggaatctgccggctgatctggcgtggtttaaacgtaacactctgga caagccggtcattatgggccgccatacgtgggaaagcatcggtcgtccgctgccgggtc

SEQ ID NO:9	gcaaaaatattatcctgagcagccagccgggcaccgatgaccgtgtgacgtgggttaa gagcgtcgatgaagcaattgcggcggcaggcgacgtgccggaaattatggttatcggc ggtggccgcgtttatgaacagttcctgccgaaagcccaaaagctgtacctgacccatat cgatgcagaagtcgaaggtgatacgcactttccggactatgaaccggatgactgggaa agtgtgttctccgaatttcacgacgccgacgctcagaacagccactcatactcattcgaa atcctggaacgccgtGGCAGCAGTACTCGAGCGAAAGAAACCGCGGCG GCGAAATTTGAACGCCAGCATATGGATAGCGGCAGCGCGAAAATT GCCGCACTTAAACAAAAAATCGCGGCGCTGAAGTATAAAAATGCGG CACTAAAAAAGAAGATTGCGGCCCTAAAACAGGGCAGCGCGTGGA GCCATCCGCAGTTTGAAAAATGATAAGCTTGGA
> DHFR$_{10+}$ (protein sequence, additional amino acid residues are underlined) SEQ ID NO:10	MASAMISLIAALAVDRVIGMENAMPWNLPADLAWFKRNTLDKPVIMG RHTWESIGRPLPGRKNIILSSQPGTDDRVTWVKSVDEAIAAAGDVPEI MVIGGGRVYEQFLPKAQKLYLTHIDAEVEGDTHFPDYEPDDWESVFS EFHDADAQNSHSYSFEILERRGSSTRAKETAAAKFERQHMDSGSAKI AALKQKIAALKYKNAALKKKIAALKQGSAWSHPQFEK**
DHFR10+ SEQ ID NO:11	ERRGSSTRAKETAAAKFERQHMDSGSAKIAALKQKIAALKYKNAALK KKIAALKQGSAWSHPQFEK
DHFRtag SEQ ID NO:12	ERRGSSTRAKKKIAALKQGSAWSHPQFEK
DHFR4+ SEQ ID NO:13	ERRGSSTRAKKIAALKQGSAWSHPQFEK
DHFR SEQ ID NO:14	ERRGSSTRAGSAWSHPQFEK
C-terminus of DHFR	ERR
S-tag SEQ ID NO:16	KETAAAKFERQHMDS
Positive coil SEQ ID NO:17	KIAALKQKIAALKYKNAALKKKIAALKQ
Strep-tag SEQ ID NO:18	WSHPQFEK
Flexible linker 1 SEQ ID NO:19	GSSTRA
Flexible linker 2 SEQ ID NO:20	GSA
Flexible linker 3 SEQ ID NO:21	GSSTRAGSA

CLAIMS

1. A method for detecting an analyte in a sample, comprising the steps of:
a) obtaining a nanopore sensor comprising a nanopore and a protein adaptor internalized in the lumen of the nanopore, wherein the protein adaptor is a functional enzyme or a ligand-binding protein,
b) adding a sample comprising an analyte to the *cis* side or the *trans* side of the nanopore, and
c) measuring conductance across the nanopore, wherein a change in conductance after addition of the sample indicates the binding of the analyte to the protein adaptor and the presence of the analyte in the sample.

2. The method according to claim 1, wherein the nanopore has a first and a second opening whereby the first opening has a wider diameter than the second opening.

3. The method according to claim 1 or 2, wherein the nanopore is cytolysin A (ClyA) or a mutant or variant thereof.

4. The method according to claim 3, wherein the cytolysin A (ClyA) mutant is Gln56Trp.

5. The method according to claim 3, wherein ClyA comprises a plurality of subunits, each subunit comprising an amino acid sequence represented by SEQ ID NO:3.

6. The method according to any one of claims 1 to 5, wherein the protein adaptor is globular.

7. The method according to any one of claims 1 to 6, wherein the protein adaptor is a demethylase enzyme or a reductase enzyme.

8. The method according to claim 7, wherein the demethylase is AlkB demethylase.

9. The method according to claim 8, wherein the demethylase is AlkB demethylase comprising an Asn120Asp mutation.

10. The method according to claim 7, wherein the reductase is dihydrofolate reductase.

11. The method according to any one of claims 1 to 10, wherein the protein adaptor comprises a tag.

12. The method according to claim 11, wherein the tag has a net overall positive or net overall negative charge.

13. The method according to any one of claims 1 to 12, wherein the protein adaptor forms a complex with one or more additional molecules.

14. The method according to any one of claims 1 to 13, wherein the analyte is a small molecule, a protein, or a nucleic acid.

15. The method according to any one of claims 1 to 14, wherein the analyte is charged.

16. A nanopore sensor comprising a nanopore and a protein adaptor internalized in the lumen of the nanopore, wherein the protein adaptor is a functional enzyme or ligand-binding protein.

17. The nanopore sensor according to claim 16, wherein the nanopore has a first and a second opening wherein the first opening in the nanopore has a wider diameter than the second opening in the nanopore.

18. The nanopore sensor according to claim 16 or claim 17, wherein the nanopore sensor is cytolysin A (ClyA) or a mutant or variant thereof.

19. The nanopore sensor according to claim 18, wherein the cytolysin A (ClyA) mutant is Gln56Trp.

20. The nanopore sensor according to claim 18, wherein ClyA comprises a plurality of subunits, each subunit comprising an amino acid sequence represented by SEQ ID NO:3.

21. The nanopore sensor according to any one of claims 16 to 20, wherein the protein adaptor is globular.

22. The nanopore sensor according to any one of claims 16 to 21, wherein the protein adaptor is a demethylase enzyme or a reductase enzyme.

23. The nanopore sensor according to claim 22, wherein the demethylase is AlkB demethylase.

24. The nanopore sensor according to 23, wherein the demethylase is AlkB demethylase comprising an Asn120Asp mutation.

25. The nanopore sensor according to claim 22, wherein the reductase is dihydrofolate reductase.

26. The nanopore sensor according to any one of claims 16-25, wherein the protein adaptor comprises a tag.

27. The nanopore sensor according to claim 26, wherein the tag has a net overall positive charge or a net overall negative charge.

28. Use of a nanopore sensor according to any one of claims 16 to 27, for the detection of an analyte in a sample.

29. The use according to claim 28, wherein the analyte is a small molecule, a protein, or a nucleic acid.

30. The use according to claim 28 or 29, wherein the analyte is charged.

A

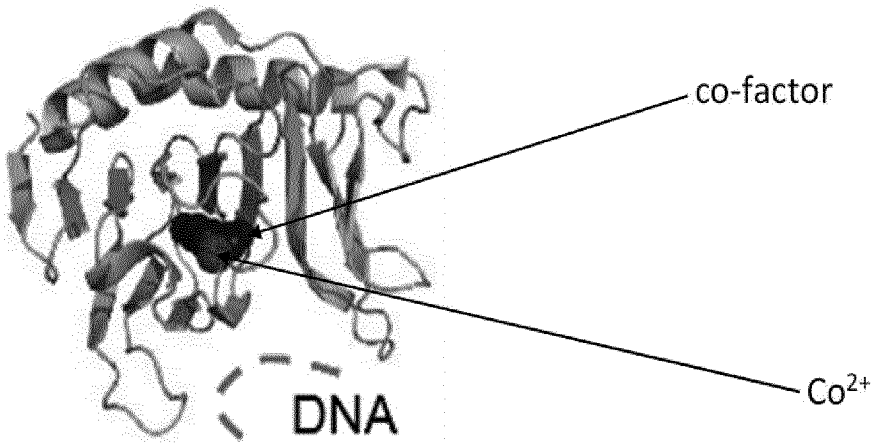
co-factor
Co^{2+}
DNA

B

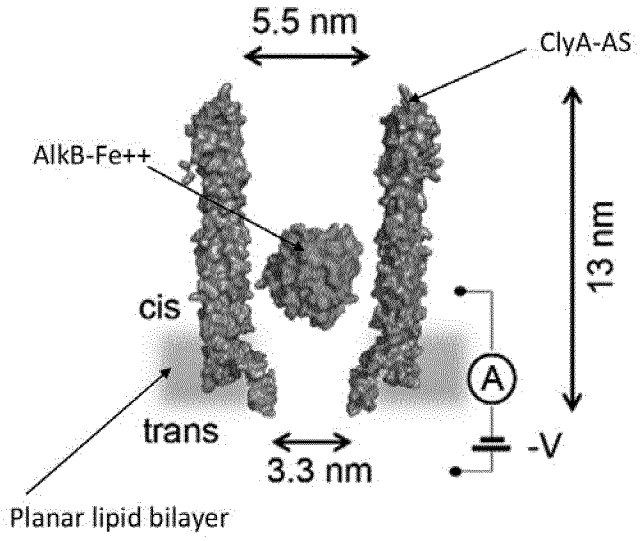
5.5 nm
ClyA-AS
AlkB-Fe++
13 nm
cis
A
trans
-V
3.3 nm
Planar lipid bilayer

Figure 1

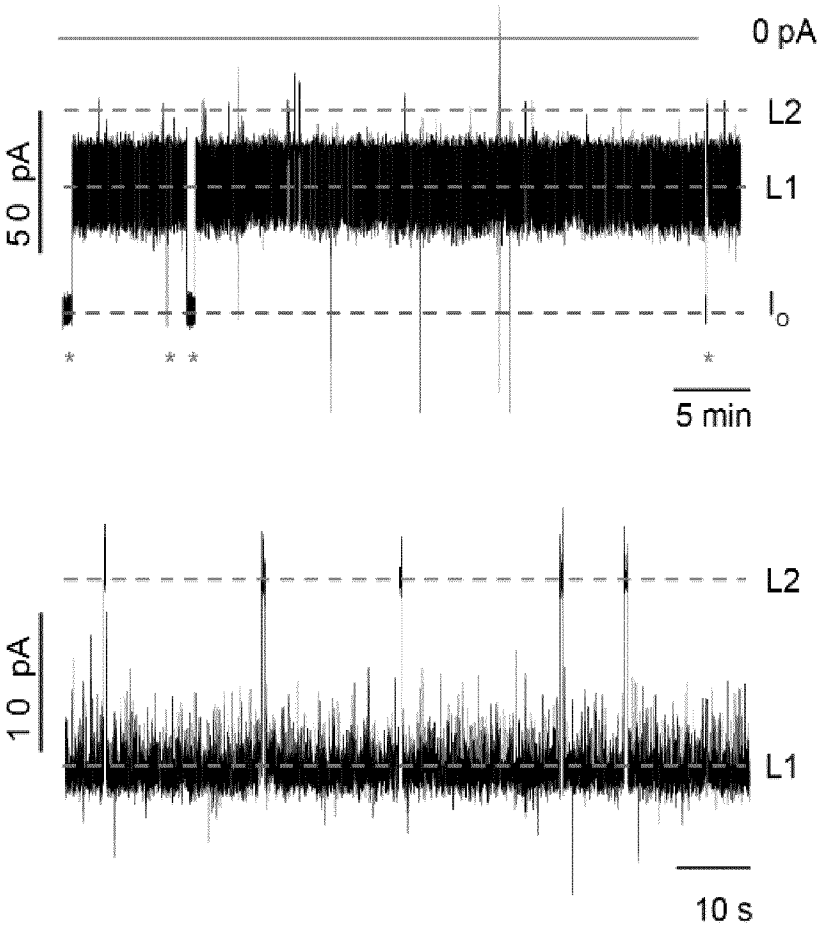

Figure 1 (continued)

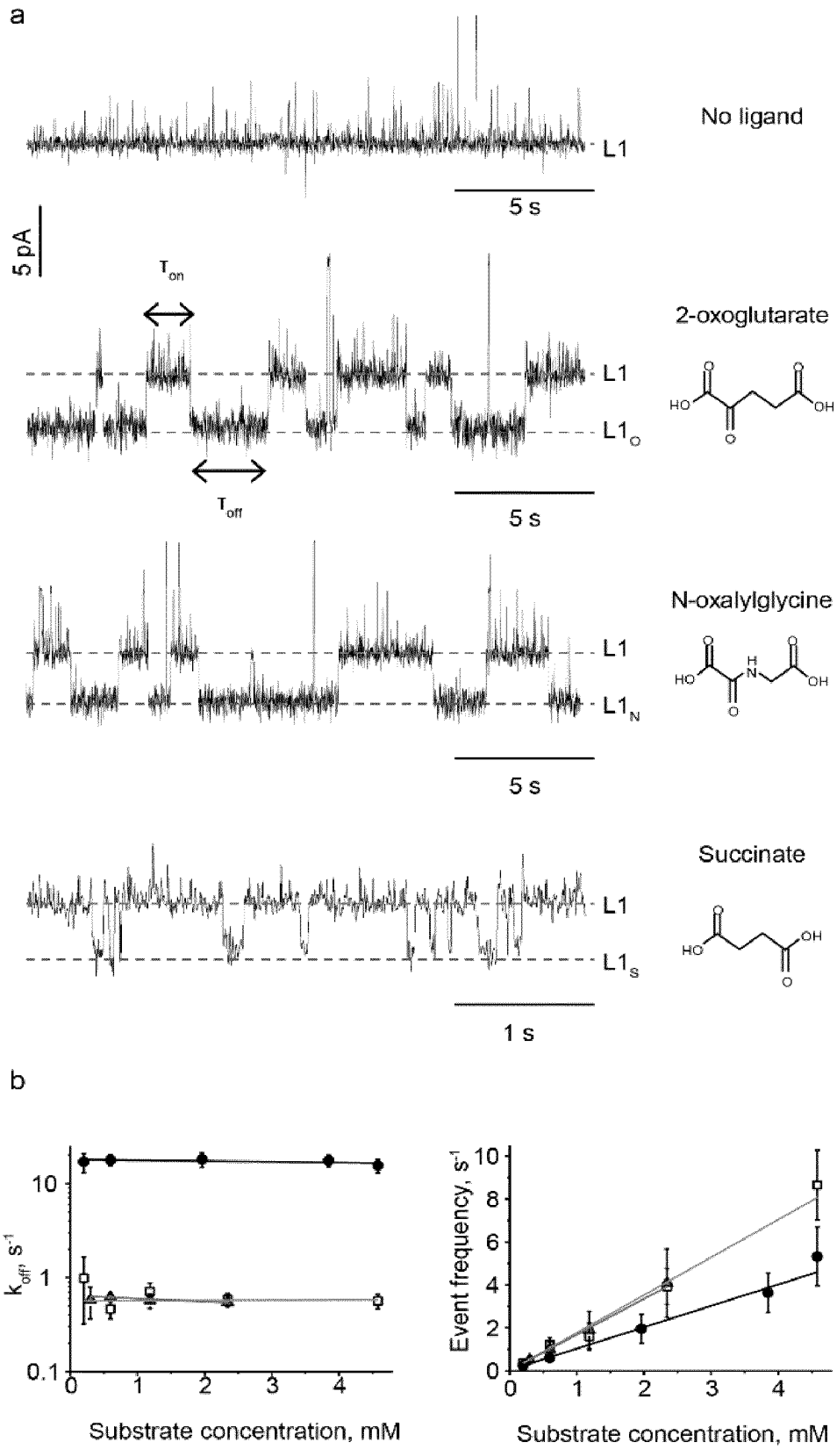
a
No ligand
L1
5 s
5 pA
T_{on}
T_{off}
2-oxoglutarate
$L1_O$
N-oxalylglycine
$L1_N$
Succinate
$L1_S$
1 s
b
k_{off}, s^{-1}
Substrate concentration, mM
Event frequency, s^{-1}
Substrate concentration, mM

Figure 2

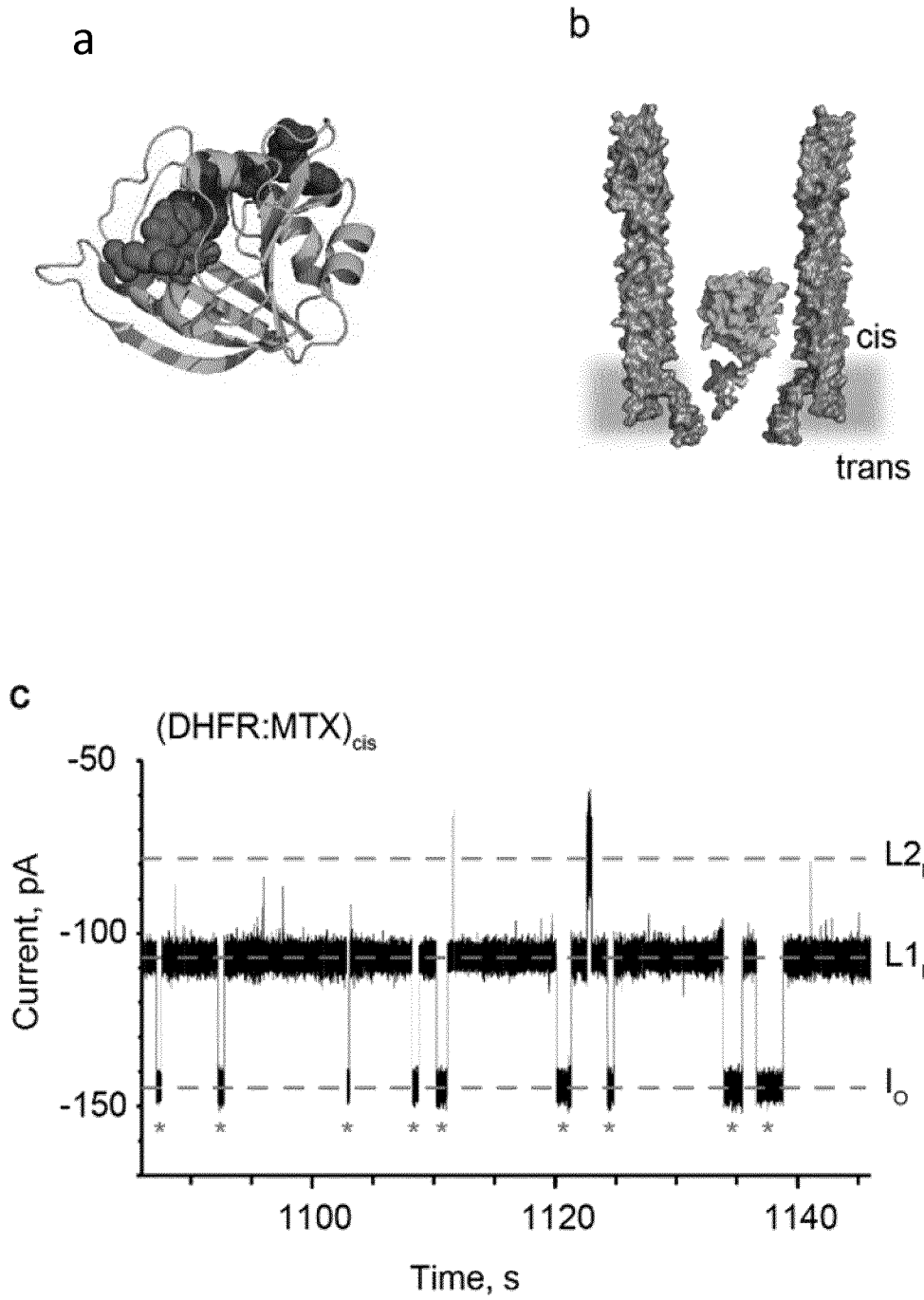
a
b
cis
trans
c
(DHFR:MTX)cis
-50
-100
-150
Current, pA
L2M
L1M
IO
1100
1120
1140
Time, s

Figure 3

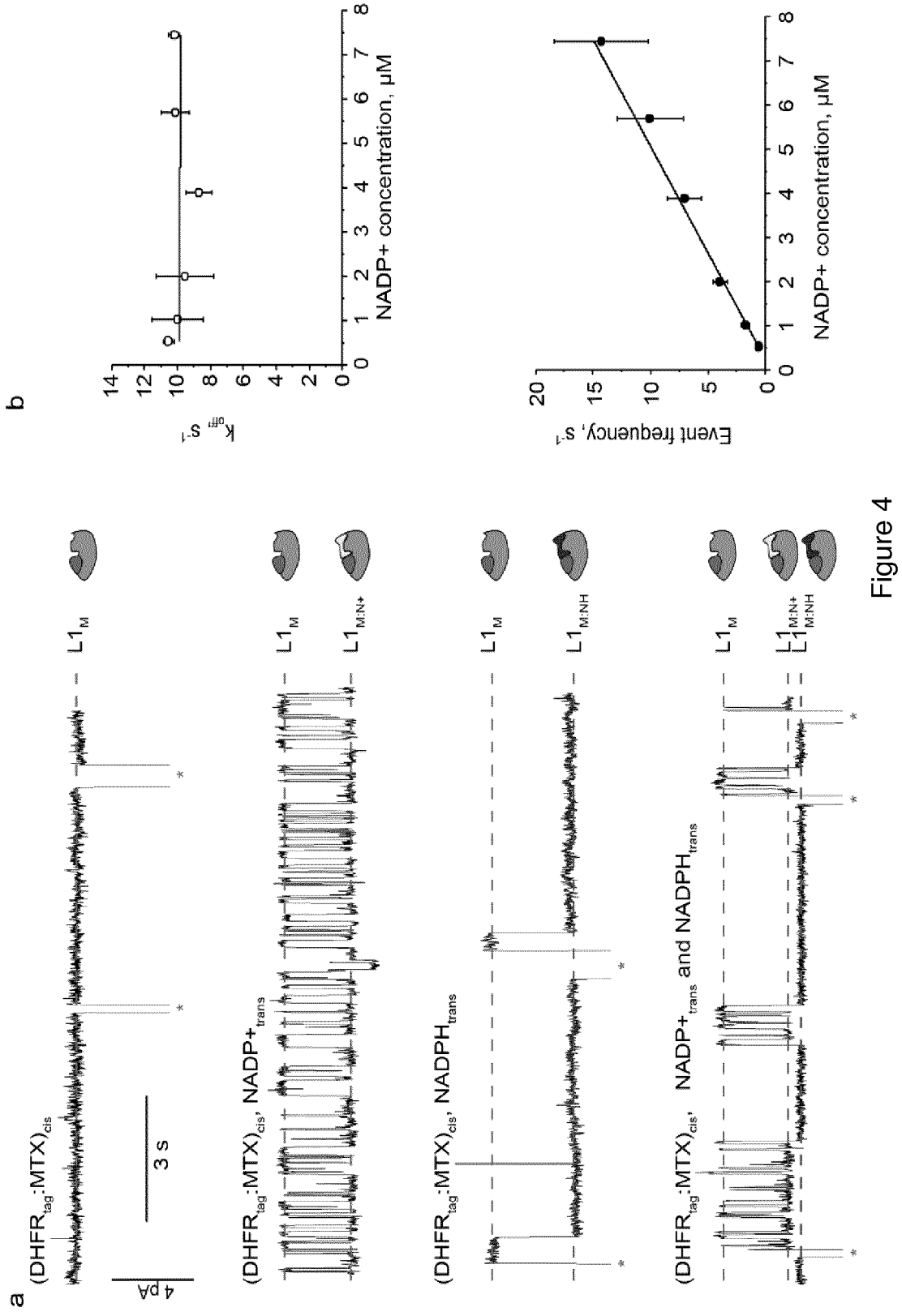
a
(DHFR$_{tag}$:MTX)$_{cis}$
L1$_M$
4 pA
3 s
(DHFR$_{tag}$:MTX)$_{cis}$, NADP+$_{trans}$
L1$_{M:N+}$
(DHFR$_{tag}$:MTX)$_{cis}$, NADPH$_{trans}$
L1$_{M:NH}$
(DHFR$_{tag}$:MTX)$_{cis}$, NADP+$_{trans}$ and NADPH$_{trans}$
b
k_{off}, s^{-1}
NADP+ concentration, µM
Event frequency, s^{-1}
NADP+ concentration, µM

Figure 4

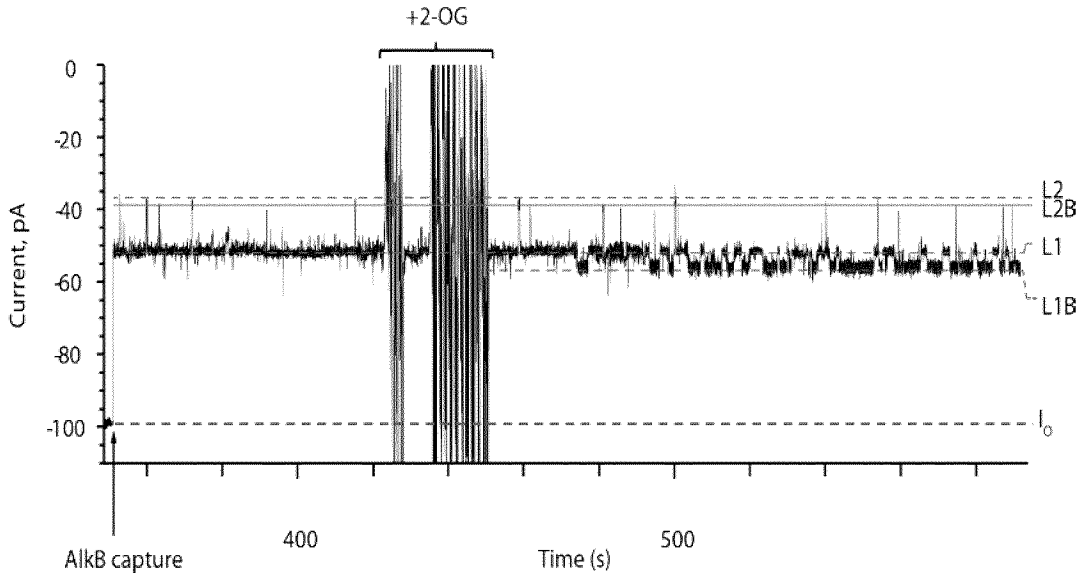

Figure 5

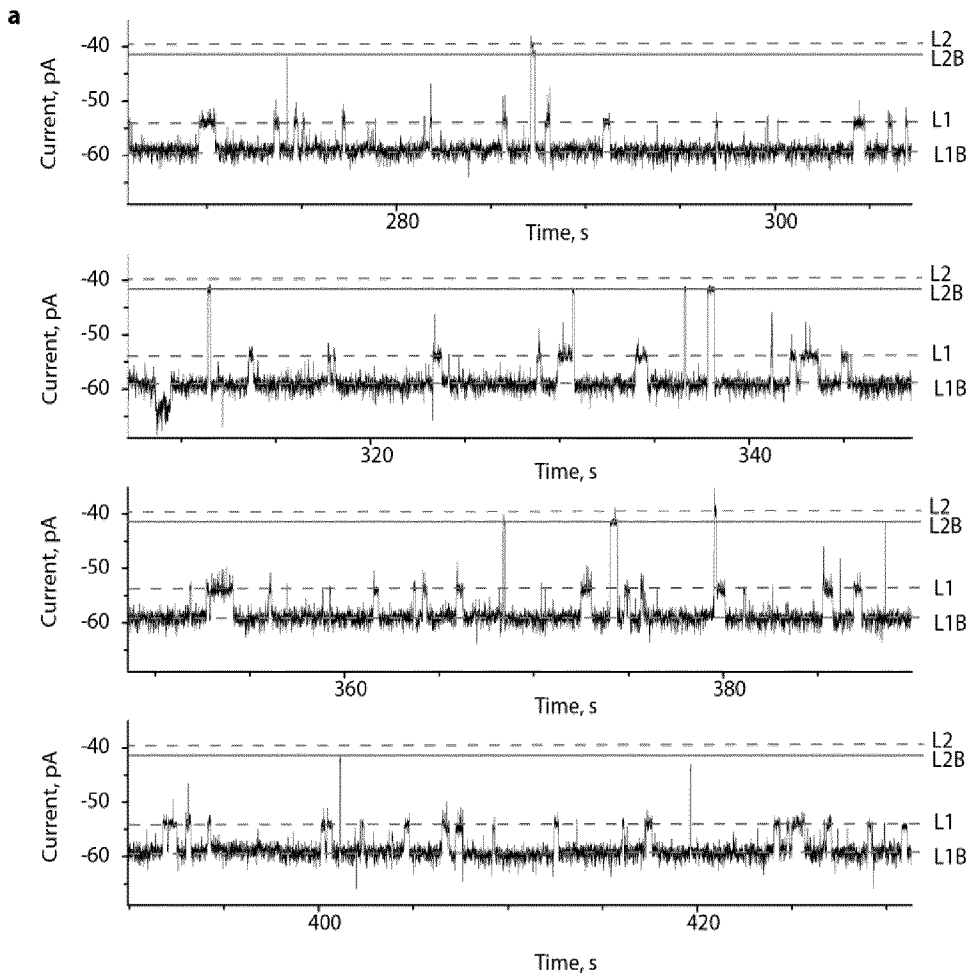

Figure 6

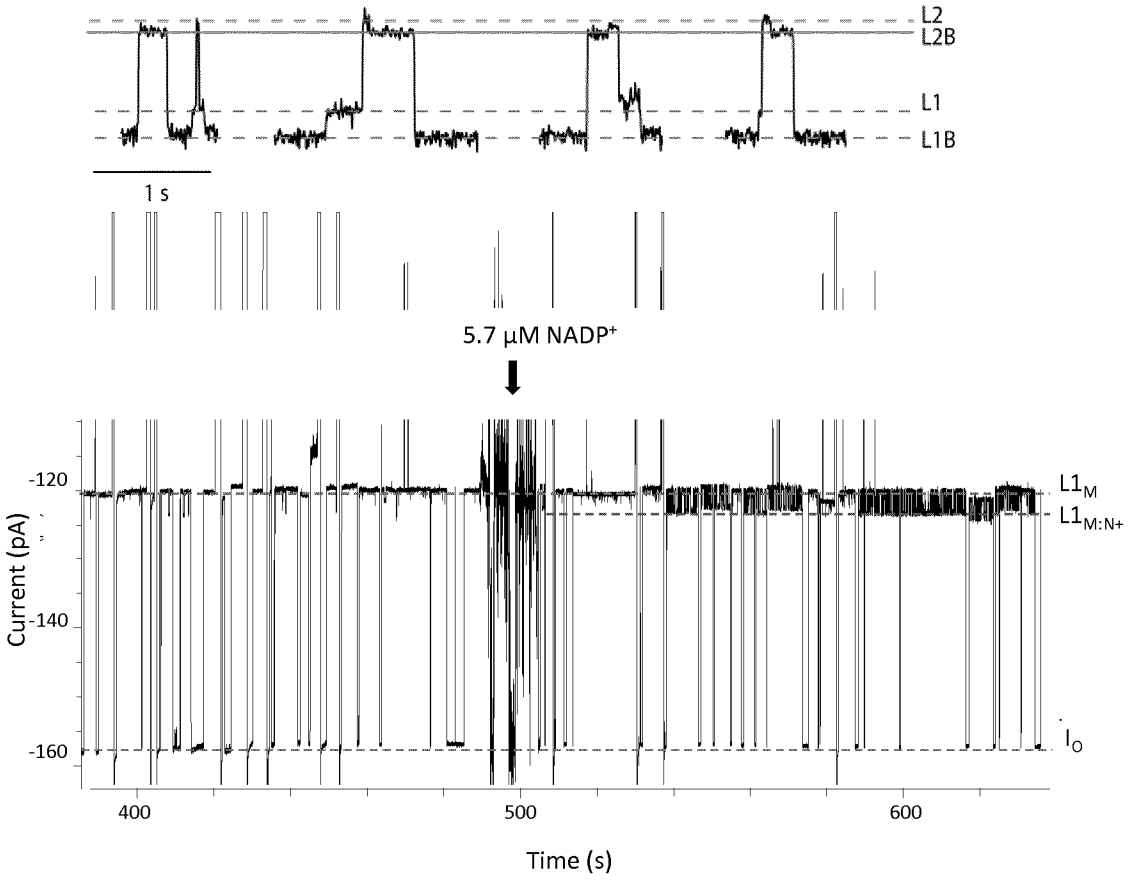

Figure 7

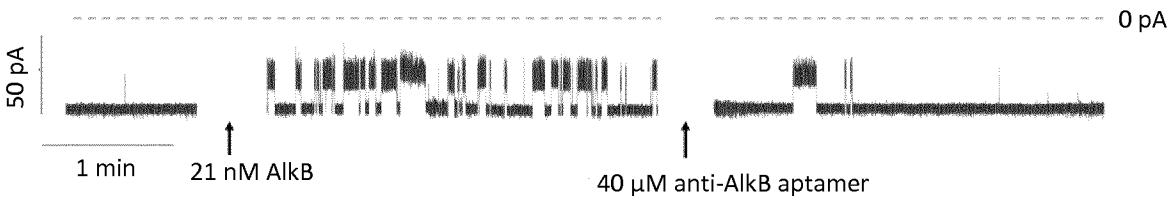

Figure 8

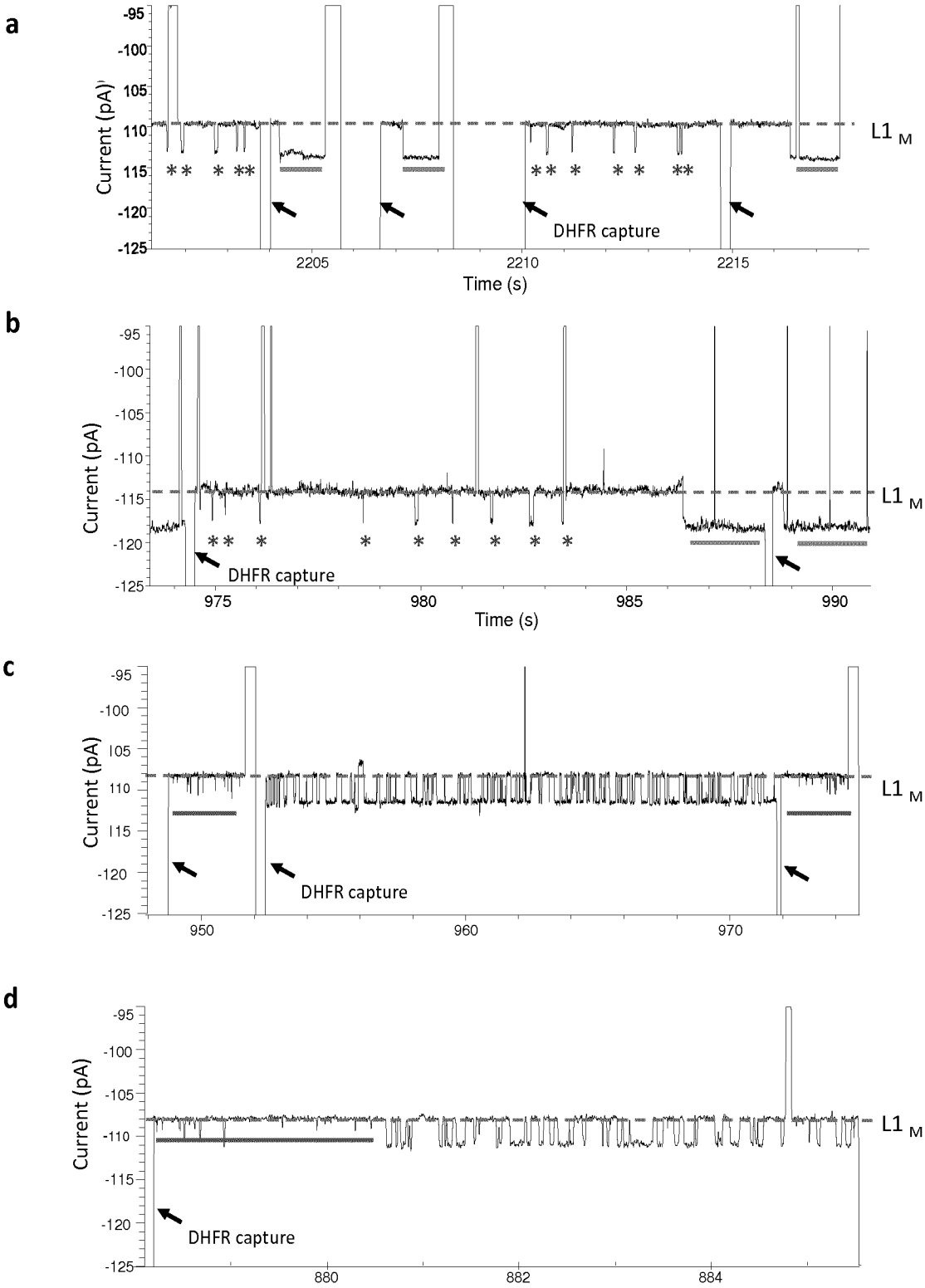
a
-95
-100
105
110
115
-120
-125
Current (pA)
L1 M
DHFR capture
2205
2210
2215
Time (s)
b
-95
-100
-105
-110
-115
-120
-125
Current (pA)
L1 M
DHFR capture
975
980
985
990
Time (s)
c
-95
-100
105
110
115
-120
-125
Current (pA)
L1 M
DHFR capture
950
960
970
d
-95
-100
-105
-110
-115
-120
-125
Current (pA)
L1 M
DHFR capture
880
882
884

Figure 9

>DHFR$_{10+}$ (SEQ ID NO:11)

```
        * *_    * _*   _    *    * *    * *    ***    *
ERRGSSTRAKETAAAKFERQHMDSGSAKIAALKQKIAALKYKNAALKKKIAALKQGSAWSHPQF
_*
EK**
```

>DHFR$_{tag}$ (SEQ ID NO:12)

```
        * ***    *          _*
ERRGSSTRAKKKIAALKQGSAWSHPQFEK**
```

>DHFR$_{4+}$ (SEQ ID NO:13)

```
        * **    *          _*
ERRGSSTRAKKIAALKQGSAWSHPQFEK**
```

>DHFR (SEQ ID NO:14)

```
        *          _*
ERRGSSTRAGSAWSHPQFEK**
```

Figure 10

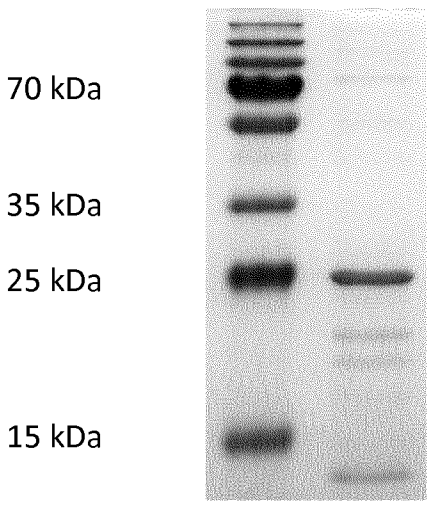

Figure 12

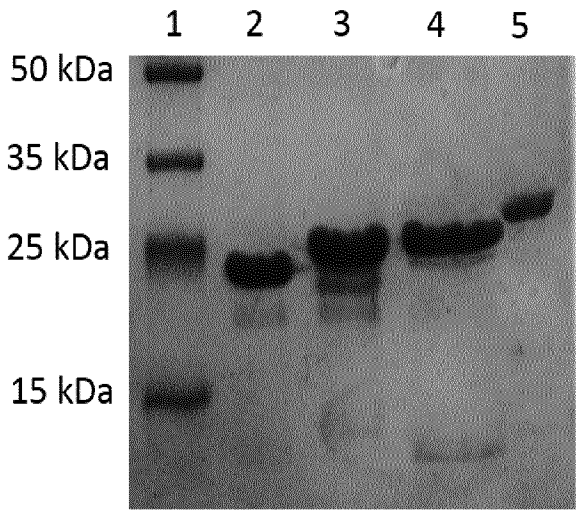

Figure 13

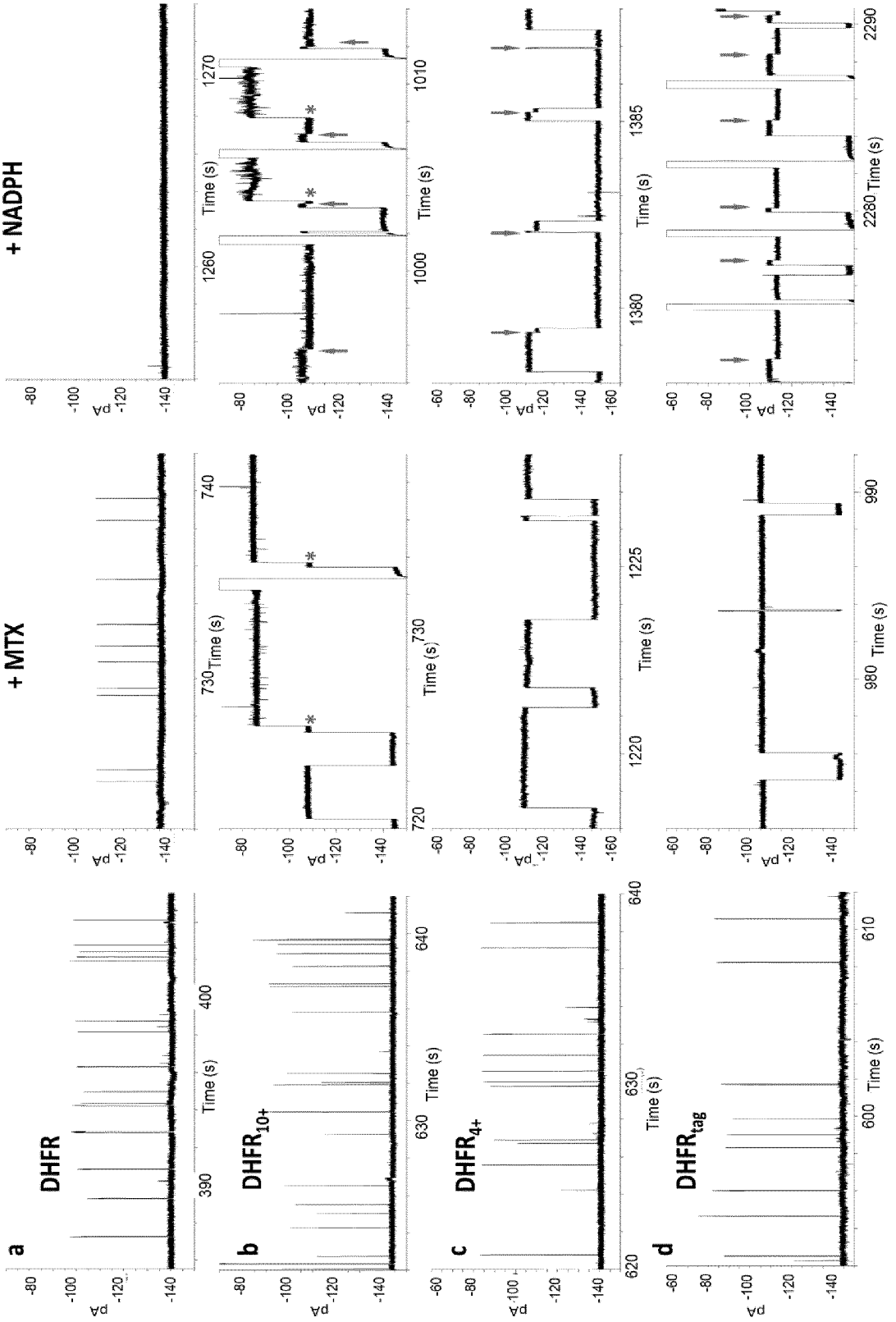

Figure 11

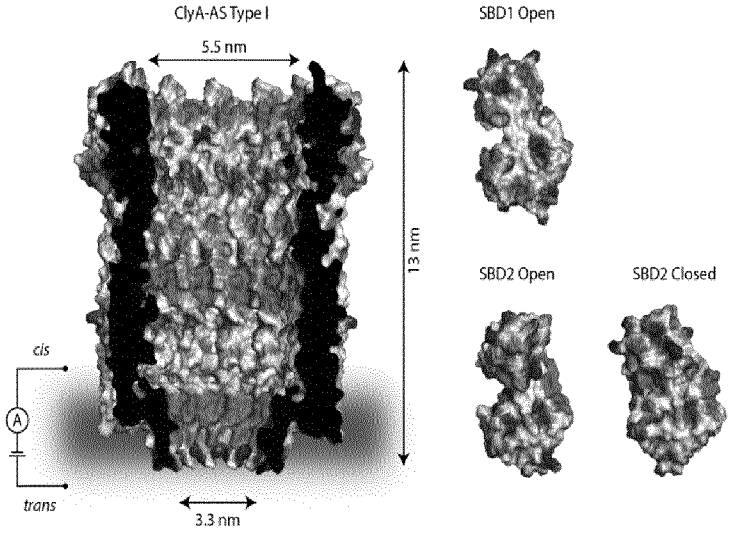

Figure 14

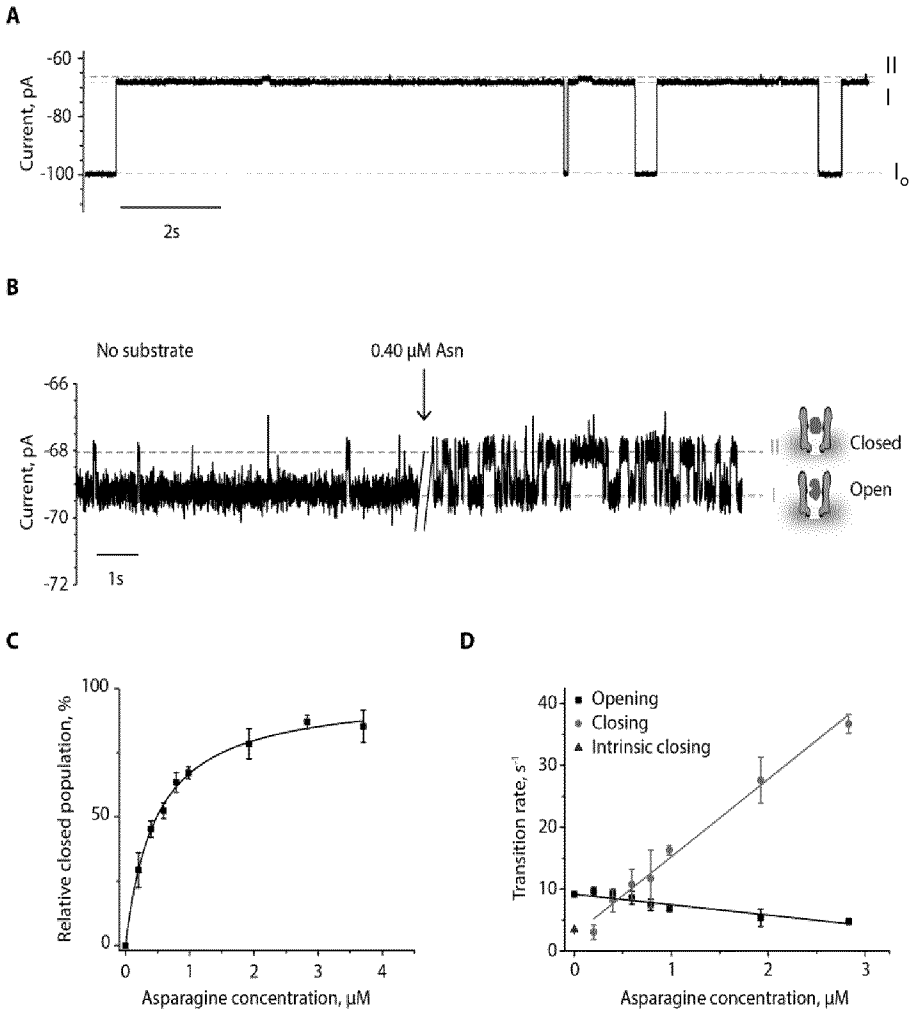

Figure 15

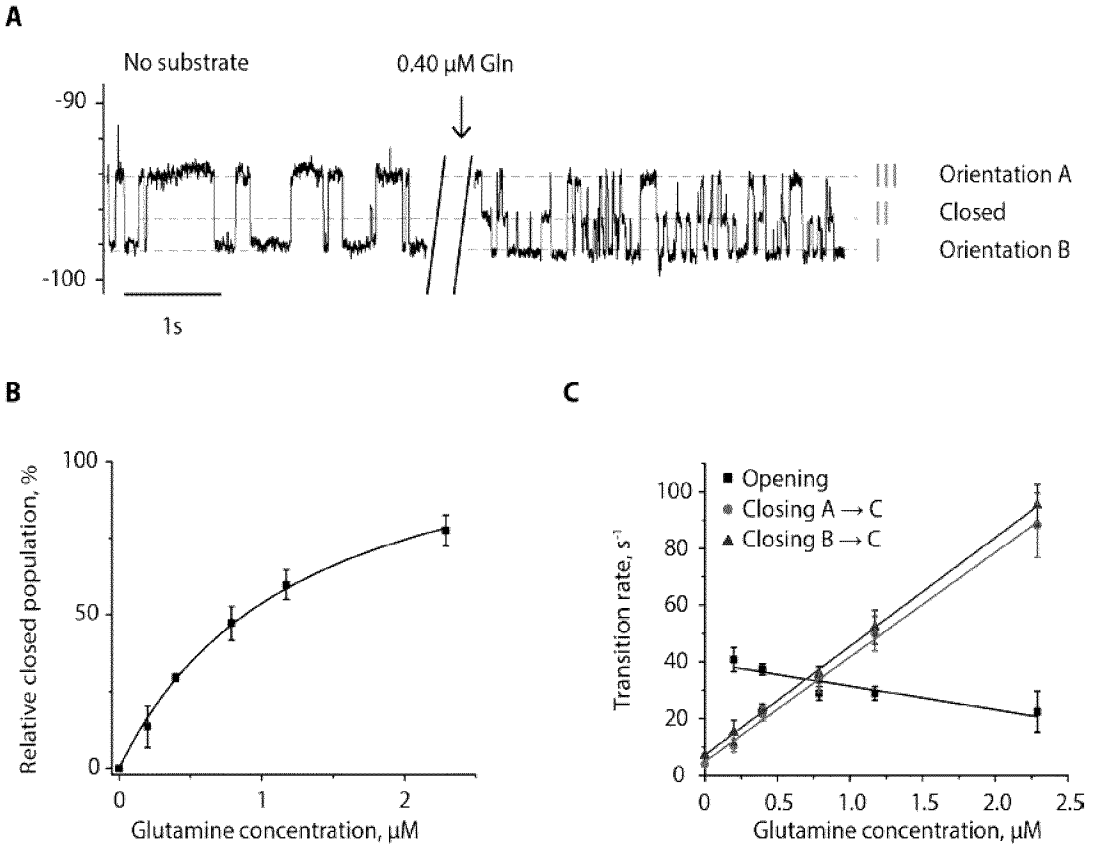

Figure 16

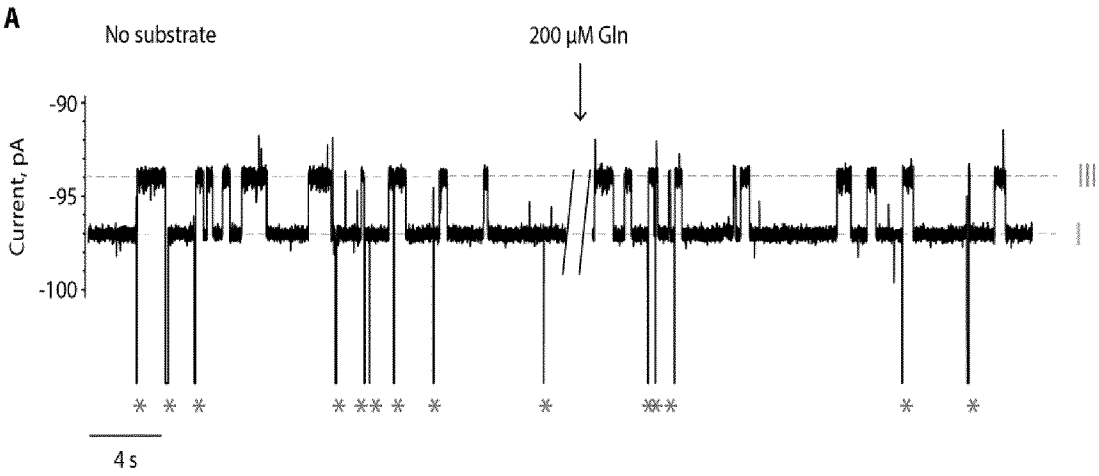

Figure 17

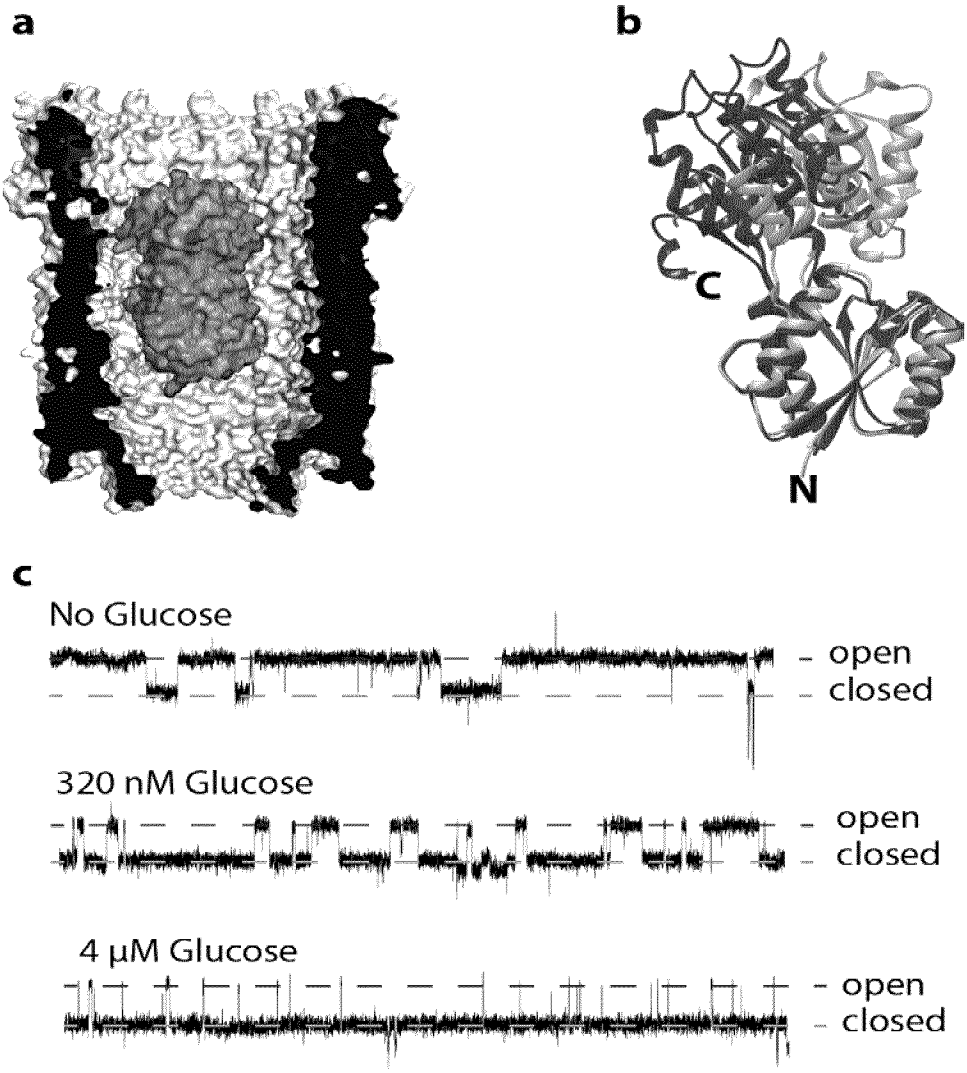
a
b
C
N
c
No Glucose
open
closed
320 nM Glucose
open
closed
4 µM Glucose
open
closed

Figure 18

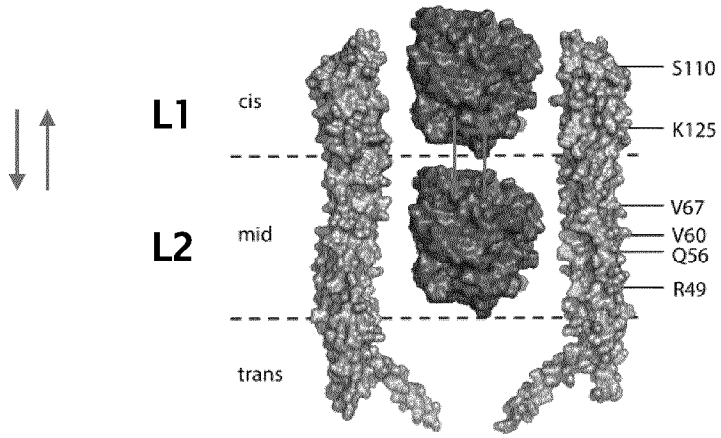

A

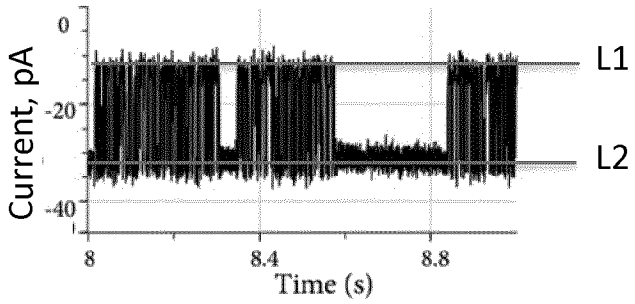

B

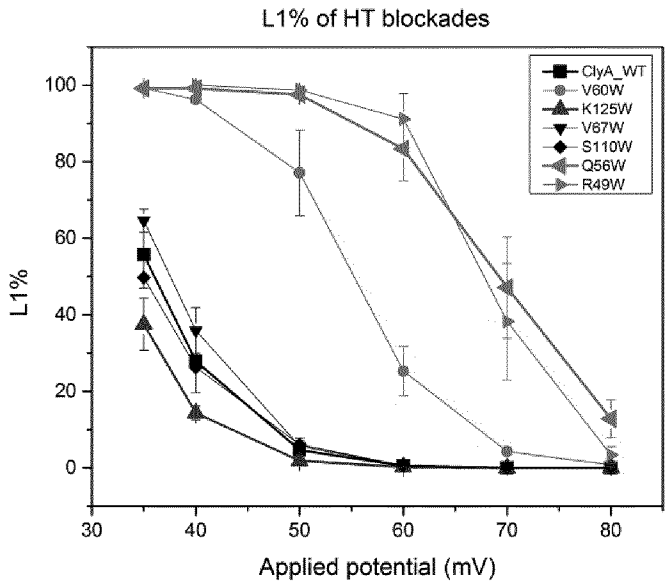

C

Figure 19

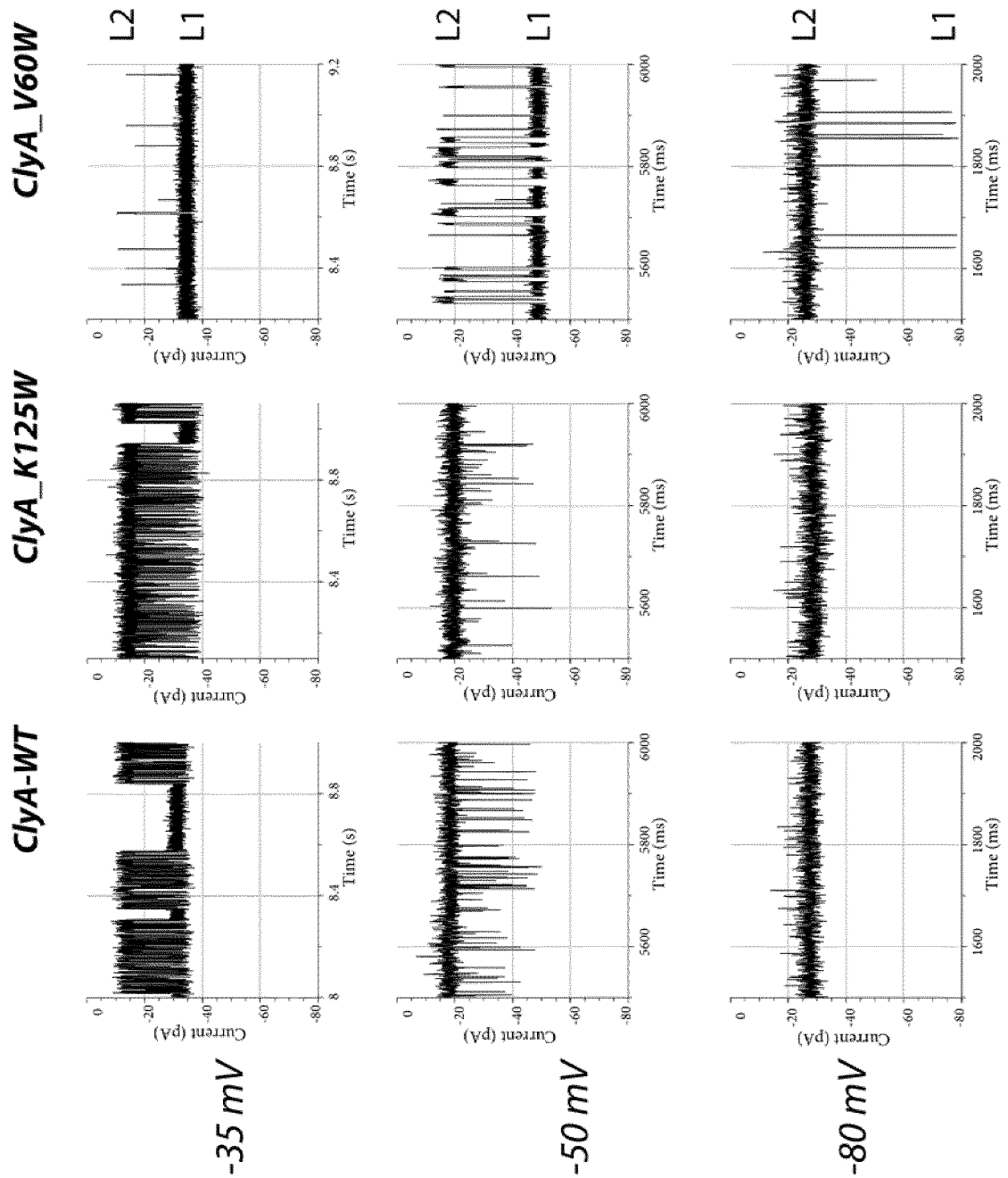
ClyA-WT
ClyA_K125W
ClyA_V60W
L2
L1
-35 mV
-50 mV
-80 mV
Current (pA)
Time (s)
Time (ms)

Figure 20

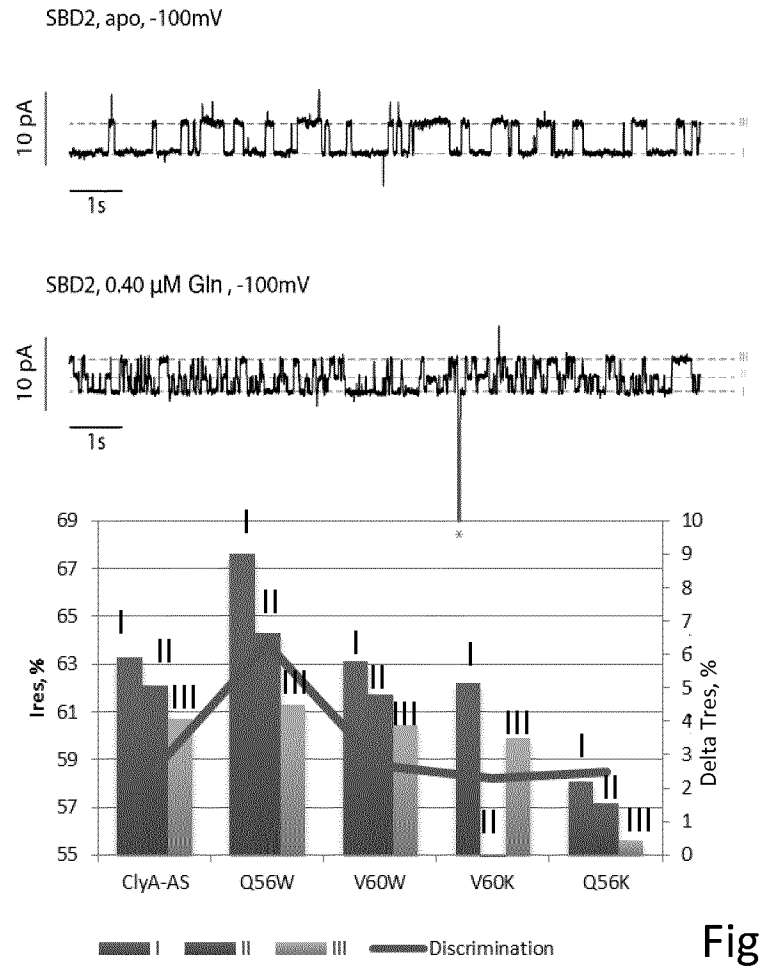

Figure 21

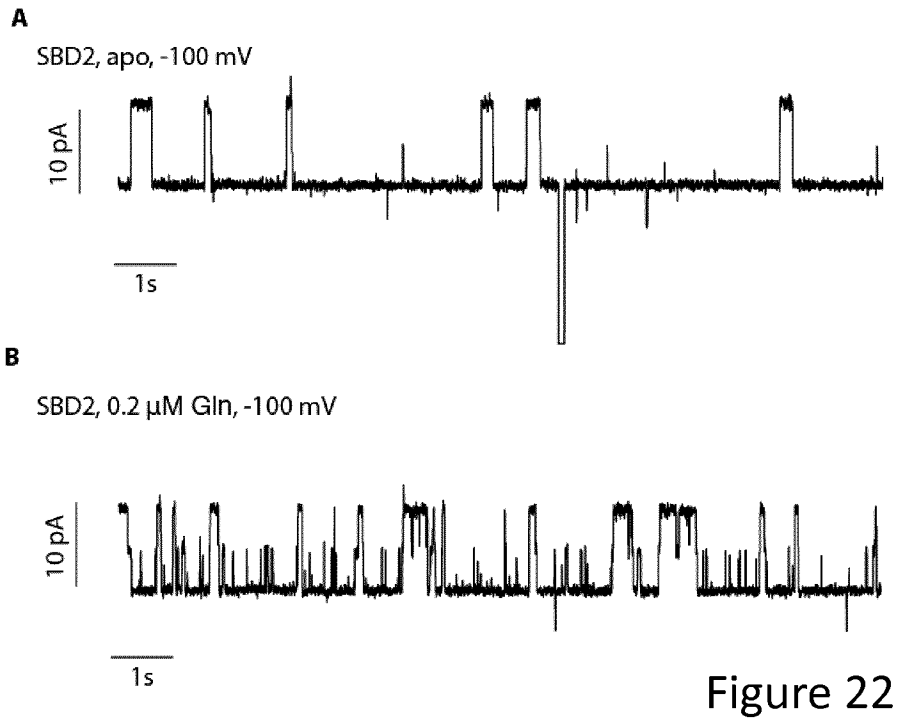

Figure 22

INTERNATIONAL SEARCH REPORT

International application No.
PCT/EP2016/058252

Box No. I Nucleotide and/or amino acid sequence(s) (Continuation of item 1.c of the first sheet)

1. With regard to any nucleotide and/or amino acid sequence disclosed in the international application, the international search was carried out on the basis of a sequence listing:

   a. [X] forming part of the international application as filed:

      [X] in the form of an Annex C/ST.25 text file.

      [ ] on paper or in the form of an image file.

   b. [ ] furnished together with the international application under PCT Rule 13*ter*.1(a) for the purposes of international search only in the form of an Annex C/ST.25 text file.

   c. [ ] furnished subsequent to the international filing date for the purposes of international search only:

      [ ] in the form of an Annex C/ST.25 text file (Rule 13*ter*.1(a)).

      [ ] on paper or in the form of an image file (Rule 13*ter*.1(b) and Administrative Instructions, Section 713).

2. [ ] In addition, in the case that more than one version or copy of a sequence listing has been filed or furnished, the required statements that the information in the subsequent or additional copies is identical to that forming part of the application as filed or does not go beyond the application as filed, as appropriate, were furnished.

3. Additional comments:

INTERNATIONAL SEARCH REPORT

International application No
PCT/EP2016/058252

A. CLASSIFICATION OF SUBJECT MATTER
INV. G01N33/68 G01N33/487
ADD.

According to International Patent Classification (IPC) or to both national classification and IPC

B. FIELDS SEARCHED

Minimum documentation searched (classification system followed by classification symbols)
G01N

Documentation searched other than minimum documentation to the extent that such documents are included in the fields searched

Electronic data base consulted during the international search (name of data base and, where practicable, search terms used)
EPO-Internal, WPI Data, BIOSIS, EMBASE, FSTA

C. DOCUMENTS CONSIDERED TO BE RELEVANT

Category*	Citation of document, with indication, where appropriate, of the relevant passages	Relevant to claim No.
X	WO 01/59453 A2 (TEXAS A & M UNIV SYS [US]) 16 August 2001 (2001-08-16) pages 1,6-8,22	1,2,6, 11-17, 21,26-30
X	WO 2014/122654 A2 (YISSUM RES DEV CO [IL]) 14 August 2014 (2014-08-14) pages 3,6,25	1,2, 11-14, 16,17, 26-30
X	WO 2014/153047 A1 (UNIV BOSTON [US]) 25 September 2014 (2014-09-25) paragraphs [0018], [0035], [0043]	1,2,6, 11,12, 14-17, 21,26, 27,29,30

-/--

[X] Further documents are listed in the continuation of Box C.

[X] See patent family annex.

* Special categories of cited documents :

"A" document defining the general state of the art which is not considered to be of particular relevance

"E" earlier application or patent but published on or after the international filing date

"L" document which may throw doubts on priority claim(s) or which is cited to establish the publication date of another citation or other special reason (as specified)

"O" document referring to an oral disclosure, use, exhibition or other means

"P" document published prior to the international filing date but later than the priority date claimed

"T" later document published after the international filing date or priority date and not in conflict with the application but cited to understand the principle or theory underlying the invention

"X" document of particular relevance; the claimed invention cannot be considered novel or cannot be considered to involve an inventive step when the document is taken alone

"Y" document of particular relevance; the claimed invention cannot be considered to involve an inventive step when the document is combined with one or more other such documents, such combination being obvious to a person skilled in the art

"&" document member of the same patent family

Date of the actual completion of the international search	Date of mailing of the international search report
30 June 2016	15/07/2016

Name and mailing address of the ISA/	Authorized officer
European Patent Office, P.B. 5818 Patentlaan 2 NL - 2280 HV Rijswijk Tel. (+31-70) 340-2040, Fax: (+31-70) 340-3016	Lunter, Pim

1

Form PCT/ISA/210 (second sheet) (April 2005)

INTERNATIONAL SEARCH REPORT

International application No
PCT/EP2016/058252

C(Continuation). DOCUMENTS CONSIDERED TO BE RELEVANT

Category*	Citation of document, with indication, where appropriate, of the relevant passages	Relevant to claim No.
X	SANCHEZ-QUESEDA J ET AL: "Cyclic Peptides as Molecular Adapters for a Pore-Forming Protein", JOURNAL OF THE AMERICAN CHEMICAL SOCIETY, AMERICAN CHEMICAL SOCIETY, US, vol. 122, no. 48, 6 December 2000 (2000-12-06), pages 11757-11766, XP002903604, ISSN: 0002-7863, DOI: 10.1021/JA002436K abstract; figure 1 -----	1,2,11, 12,14, 16,17, 26-30
X	SOSKINE M ET AL: "An engineered ClyA nanopore detects folded target proteins by selective external association and pore entry", NANO LETTERS, AMERICAN CHEMICAL SOCIETY, US, vol. 12, no. 9, 12 September 2012 (2012-09-12), pages 4895-4900, XP002727575, ISSN: 1530-6984, DOI: 10.1021/NL3024438 [retrieved on 2012-08-06] abstract page 4896 - page 4899 -----	1-3,5,6, 11-18, 20,21, 26-30
X	MISHA SOSKINE ET AL: "Tuning the Size and Properties of ClyA Nanopores Assisted by Directed Evolution", JOURNAL OF THE AMERICAN CHEMICAL SOCIETY, AMERICAN CHEMICAL SOCIETY, US, vol. 135, no. 36, 6 August 2013 (2013-08-06), pages 13456-13463, XP002727574, ISSN: 0002-7863, DOI: 10.1021/JA4053398 [retrieved on 2013-08-06] abstract page 13456 -----	1-3,5,6, 11-18, 20,21, 26-30

1

INTERNATIONAL SEARCH REPORT

Information on patent family members

International application No
PCT/EP2016/058252

Patent document cited in search report	Publication date	Patent family member(s)	Publication date
WO 0159453 A2	16-08-2001	AU 4147401 A	20-08-2001
		EP 1255772 A2	13-11-2002
		EP 2083015 A2	29-07-2009
		EP 2261240 A2	15-12-2010
		US 2002094526 A1	18-07-2002
		US 2005208574 A1	22-09-2005
		WO 0159453 A2	16-08-2001
WO 2014122654 A2	14-08-2014	CN 105074458 A	18-11-2015
		EP 2954320 A2	16-12-2015
		US 2015354001 A1	10-12-2015
		WO 2014122654 A2	14-08-2014
WO 2014153047 A1	25-09-2014	US 2016033471 A1	04-02-2016
		WO 2014153047 A1	25-09-2014